Pure appl. geophys. 158 (2001) 1207–1250
0033–4553/01/071207–44 $ 1.50 + 0.20/0

Pure and Applied Geophysics

Sedimentary Basins and the Blockage of *Lg* Wave Propagation in the Continents

DOUGLAS R. BAUMGARDT[1]

Abstract—The phenomenon of "*Lg* blockage," where *Lg* is strongly attenuated by crustal heterogeneities, poses a serious problem to CTBT monitoring because *Lg* is an important seismic phase for discrimination. This paper examines blockage in three continental regions where the *Lg* blockages may be caused by large, enclosed sedimentary basins along the propagation path. The Barents Sea Basin blocks *Lg* propagation across the Barents Sea from the Russian nuclear test sites at Novaya Zemlya to Scandinavian stations. Also, "early *Lg*" waves are observed in *Sn* codas on NORSAR, NORESS, and ARCESS recordings of Novaya Zemlya explosions where direct *Lg* is blocked. Early *Lg* waves may have resulted from *Sn*-to-*Lg* mode conversion at the contact between the Barents Basin and the Kola Peninsula. The Northern and Southern Caspian Sea Basins also block *Lg* waves from PNEs and earthquakes, perhaps due to thick, low-velocity, low-*Q* sediments replacing the granitic layer rocks in the crust. *Lg* blockage has also been observed in the Western Mediterranean/Levantine Basin due to low-*Q* sediments and crustal thinning. A "basin capture" model is proposed to explain *Lg* blockage in sedimentary basins. In this model, shear waves that reverberate in the crust and constitute the *Lg* wave train are captured, delayed, and attenuated by thick, low-velocity sediments that replace the "granitic" layer rocks of the upper crust along part of the propagation path. *Sn* waves, which propagate below the basin, would not be blocked and in fact, the blocked *Lg* waves may be diverted downward into *Sn* waves by the low velocity sediments in the basin.

Key words: *Lg* blockage, sedimentary basins, nuclear explosions, earthquakes, discrimination.

Introduction

The *Lg* phase has assumed critical importance in monitoring the Comprehensive Test-Ban Treaty (CTBT), especially for event identification. Recent studies in seismic discrimination have shown that explosions and earthquakes may be separable, based on the earthquakes having higher *Lg* excitation relative to *P* than explosions (BENNETT *et al.*, 1995; BAUMGARDT and YOUNG, 1990; HARTSE *et al.*, 1997; KIM *et al.*, 1997). The proper use of *Lg* amplitude measurements for seismic source characterization requires that propagation path effects on *Lg* amplitudes be understood. MURPHY *et al.* (1997), in a study of Peaceful Nuclear Explosions

[1] ENSCO, Inc., 5400 Port Royal Rd., Springfield, VA 22151, USA. Fax: 703-321-4609, E-mail: doug@ensco.com

(PNEs) in the Former Soviet Union (FSU), have observed uncharacteristically small P/Lg amplitude ratios for nuclear explosions, presumably caused by unexplained effects of heterogeneous crustal structure on regional phase propagation. Other studies have shown that laterally heterogeneous crustal structure can cause *Lg* "blockage" which makes measurements of P/Lg amplitude ratios impossible (BAUMGARDT, 1990).

The regional seismic phase identified as *Lg* is usually, but not always, the most prominent phase on regional seismograms. It has usually been interpreted as the superposition of higher-mode Rayleigh waves that primarily propagate in the crust (KNOPOFF *et al.*, 1973) and, alternatively, as the superposition of supercritically reflected shear waves in the continental crust (CAMPILLO *et al.*, 1985; KENNETT, 1986). *Lg* propagation has only been observed in the continents and does not appear to cross ocean basins or paths that contain 100 to 200 km of oceanic crust (EWING *et al.*, 1957).

The term "*Lg* blockage" refers to the sudden disappearance of the phase along a particular propagation path that crosses a geologic or tectonic structure boundary or lateral heterogeneity. Although *Lg* propagates efficiently across continental regions, *Lg* blockages have been observed in several continental areas. Explanations for the cause of *Lg* blockage include (1) Drastic variations in crustal thickness and topography, (2) scattering from tectonic boundaries, (3) strong anelastic attenuation in upper-crustal sediments, and (4) lack of an upper-crustal "granitic layer."

RUZAIKIN *et al.* (1997) proposed crustal thickness variations to explain the inefficient propagation of *Lg* in the Tibetan Plateau. The region is known to have unusually thick (up to 70 km) crust due to the convergent type tectonics of the region. KENNETT *et al.* (1985) also suggested that *Lg* propagation across the Norwegian Sea might be blocked by a region of crustal thinning beneath a graben structure. KENNETT (1986) has shown with ray-tracing modeling that *Lg* blockage can be caused by sudden crustal thinning, as might occur at a continent/ocean boundary (e.g., SHAPIRO *et al.*, 1996). The second explanation has been invoked by a number of investigators who have used the efficiency of *Lg* propagation as a method for mapping tectonic boundaries (e.g., KADINSKY-CADE *et al.*, 1981; NI and BARAZANGI, 1983). BAUMGARDT (1985, 1990) has provided evidence for *Lg* scattering in the Ural Mountains, a collisional suture zone, which partially blocks the propagation of *Lg* waves from the Semipalatinsk test site in eastern Kazakh to the ARCESS array. MITCHELL and HWANG (1987) have suggested that the attenuation of *Lg* may be strongly affected by low *Q* sediments, which are known to be present in the Barents Basin (CHAN and MITCHELL, 1985). MCNAMARA *et al.* (1996) attribute *Lg* blockage in Tibet to low *Q* and perhaps the unusually thick crust beneath the Tibetan Plateau. The "missing granitic layer" explanation originates from the idea that such a layer is essential to provide the waveguide for *Lg* propagation, a phase only observed in continental regions. PIWINSKII (1981) has explained the poor propagation of *Lg* in the Caspian Sea region of the Soviet Union

in terms of an implied "missing granitic layer" that has also been reported in the Soviet geophysical literature for the Caspian Sea sedimentary basin. Theoretical studies of CAO and MUIREHEAD (1993) and JIH (1995) show how anomalous crustal structure associated with substantial crustal thinning can cause partial *Lg* blockage. ZHANG and LAY (1995) argue that the extremely thin oceanic crust is primarily responsible for the inefficient propagation of *Lg* in the oceans.

This paper revisits this issue by reviewing data that reveals *Lg* blockages in three continental regions: the Barents Sea near the FSU test site of Novaya Zemlya, the Russian/Iranian border region, including both the northern and southern Caspian Sea, and in the Eastern Mediterranean/Levant region in the Middle East. The method used to identify the cause of *Lg* blockage is to make crustal cross sections for the blocked and unblocked paths, and to look for differences between the two paths. These crustal cross sections are derived from available databases of elevation and depth to the crystalline basement (sediment depths), and inferred and measured crustal thicknesses. This method assumes that regional phases propagate along great circle paths from source to receiver. This analysis reveals that the deep sedimentary basins in these regions may account for the *Lg* blockages. In addition to presenting the data examples of *Lg* blockage in the sedimentary basins, a mechanism to explain *Lg* blockages in sedimentary basins, called "basin capture," is presented.

The Barents Sea Sedimentary Basin

NORSAR Observations

The characteristics of regional waveforms recorded at NORSAR from several nuclear explosions have been analyzed. These include two Soviet peaceful nuclear explosions (PNEs) on the Kola Peninsula and in western Russia near the White Sea and five explosions at Novaya Zemlya. The source parameters for these explosions are given in Table 1, and the locations of the explosions and great circle paths from

Table 1

Parameters for events studied at NORSAR

Date	Time	Latitude	Longitude	m_b	Region
09/04/72	07:00:3.6	67.69	33.45	4.6	Kola Peninsula PNE
08/10/78	07:59:57.7	73.31	54.70	5.9	Novaya Zemlya
10/11/80	07:09:57.2	73.36	54.82	5.7	Novaya Zemlya
08/18/83	16:00:58.6	73.38	54.87	5.9	Novaya Zemlya
09/25/83	13:09:57.9	73.35	54.39	5.8	Novaya Zemlya
10/25/84	06:29:57.7	73.37	54.96	5.9	Novaya Zemlya
07/18/85	21:14:57.4	65.97	40.86	5.0	White Sea/ Archangel'sk PNE

the explosions to NORSAR are shown on the map in Figure 1(A). The paths from the two PNEs are entirely continental whereas the path from Novaya Zemlya to

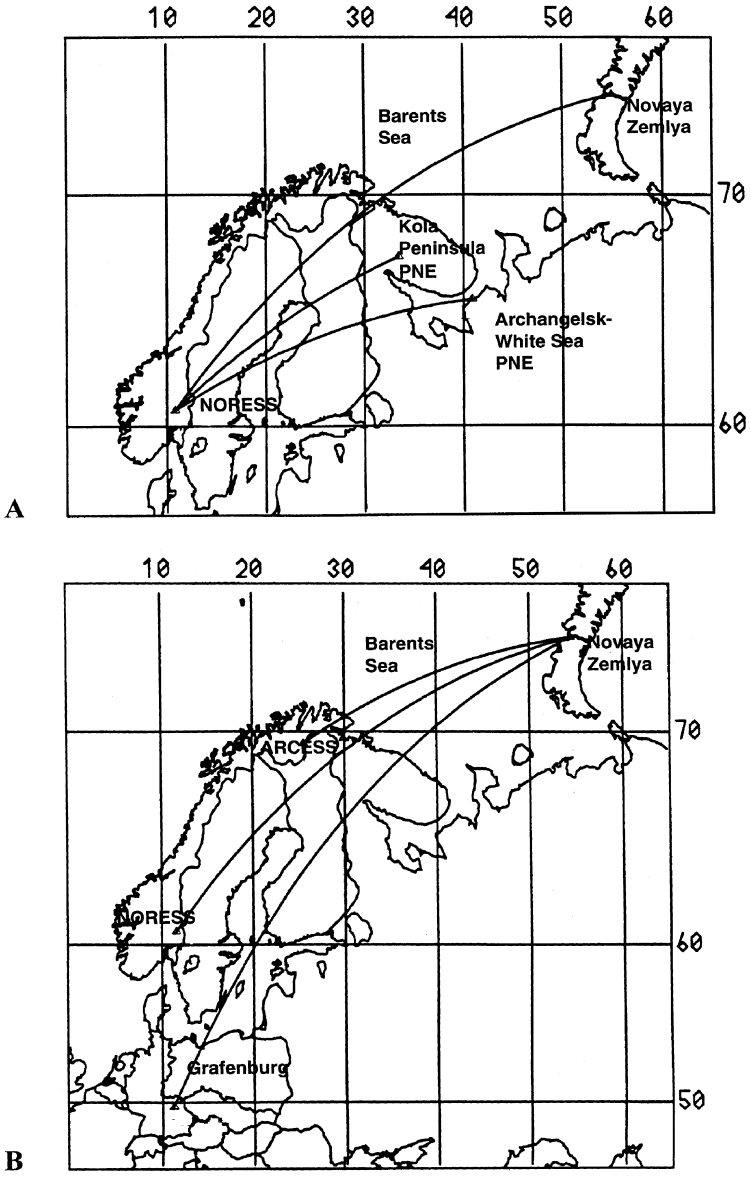

Figure 1
(A) Map showing the locations of the Kola and White Sea/Archangel'sk PNEs and the great-circle propagation paths from the Novaya Zemlya nuclear test site to the NORSAR array. (B) Map showing the great-circle propagation paths from the Novaya Zemlya test site to the ARCESS, NORESS, and Grafenburg arrays.

NORSAR has a segment that includes the Barents Sea. Thus, comparison of the *Lg* waves from the PNEs with those from Novaya Zemlya will show directly the effects of the Barents segment on the *Lg* propagation efficiency. The Novaya Zemlya explosions selected for this study registered magnitudes less than 6.0 and were not clipped at the times when *Sn* and *Lg* are expected.

Figure 2 shows a record section of the waveforms recorded at the N01A0 channel of NORSAR for the two PNEs and one of the Novaya Zemlya explosions. Each waveform has been filtered in the 0.6 to 3.0 Hz band. The arrivals identified as *Pn*, *Sn*, and *Lg* are marked on the waveforms. The two PNEs produced waveforms that resemble typical regional waveforms, with relatively sharp *Pn* onsets, an emergent arrival corresponding to the *Sn* onset, and strong *Lg* arrivals. The Novaya Zemlya explosion produced a strong *P* signal at NORSAR, an emergent *Sn* onset similar to the one from the PNEs, but no corresponding *Lg* arrival. It should be noted that the *Pn* signal from Novaya Zemlya is clipped, therefore the actual amplitude of *Pn* relative to *Sn* is actually much greater than that implied in Figure 2.

Figure 2 clearly shows that *Lg* has been greatly reduced relative to *P* for the Novaya Zemlya explosion, compared with those of the nearby PNEs. Although some

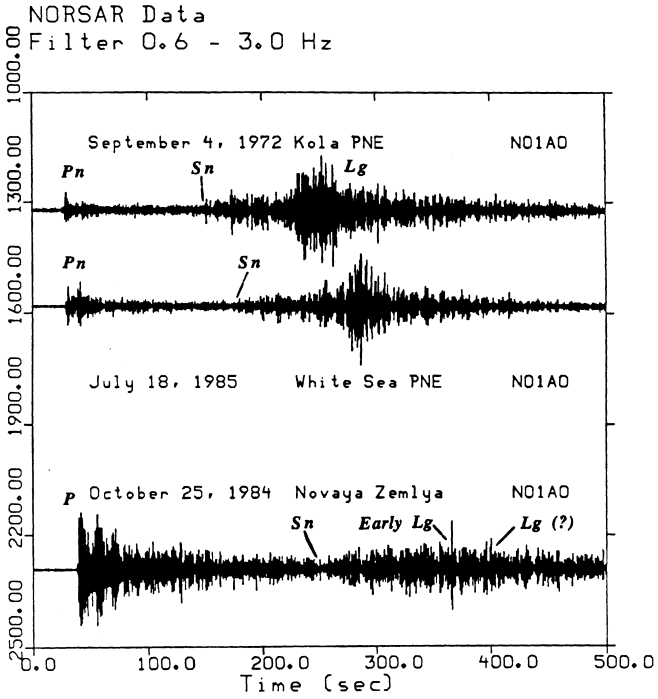

Figure 2
Record section of waveforms, recorded at the N01A0 element of the NORSAR array, from the Kola and White Sea/Archangel'sk PNEs and a Novaya Zemlya nuclear explosion. The numbers on the vertical axis denote the epicentral distance in km.

attenuation in *Lg* would be expected due to the increased distance of Novaya Zemlya from NORSAR compared with the PNEs, the lack of *Lg* from Novaya Zemlya cannot be explained by anelastic attenuation effects alone.

One notable feature of the Novaya Zemlya recording is a strong arrival that appears in the *Sn* coda well ahead of the expected 3.5 km/sec *Lg* arrival. This arrival corresponds in time to the "early *Lg*" phase discussed by BAUMGARDT (1990), that was also observed for recent Novaya Zemlya explosions recorded at NORESS. This phase was interpreted as being an *Lg* phase because its phase velocity, measured by the frequency-wavenumber (FK) method, was less than 4.0 km/sec, the value expected for *Lg*. However, its group arrival time is too early to be the *Lg* that propagates directly from Novaya Zemlya with group velocity of 3.5 km/sec.

This phase is interpreted to be an *Lg* phase produced by mode conversions of *Sn* at the interface of the Barents Sea and the Kola Peninsula, similar to those observed at coastlines in other regions for offshore events recorded on land (e.g., ISACKS and STEPHENS, 1975; BARAZANGI, 1977; CHINN *et al.*, 1980; SEBER *et al.*, 1993). The point at which the direct *Sn* from Novaya Zemlya intersects the Kola Peninsula is at a distance of about 13° from NORSAR, as shown in Figure 3(A). If *Lg* originates at that point, due to mode conversion from *Sn*, the converted *Lg* would lag the *Sn* phase by about 110 seconds, using the travel-time curve of Eurasia of GUPTA *et al.* (1980), shown in Figure 3(B). This is about the time delay between the *Sn* onset and the *Sn*-coda arrival in Figure 2.

Figure 4 shows a plot of the incoherent beams of all five Novaya Zemlya explosions recorded at NORSAR. Incoherent beams are array-stacked log-rms envelopes computed from the NORSAR vertical-component seismograms. Each trace begins after the *Pn* onset time and has been shifted vertically by one log-rms unit for display purposes, consequently the vertical axis only gives relative log-rms amplitudes. Note that the envelope traces begin after the maximum amplitude of the first arrival *P*, which is clipped on most channels, and the horizontal dashed lines show the mean noise level over two minutes ahead of the *P* onset. Each waveform was filtered from 0.6 to 3.0 Hz before the log-rms stack traces were computed.

The first solid vertical line indicates the inferred onset of *Sn*, and the vertical dashed line marks the expected arrival time of the presumed *Sn*-to-*Lg* conversion at 110 seconds after the *Sn* phase. At this time a peak is evident on the beam with log-rms amplitude above that of the maximum *Sn* amplitude. The second solid vertical line marks the inferred arrival time of the direct *Lg* phase, which should have a group velocity of 3.5 km/sec. This arrival seems to be manifested on each trace by a flattening of the coda level after the early-*Lg* onset. The signal-to-noise ratio at the time of the expected on-time *Lg* is quite large, although the *Lg* amplitude is much less than the *Sn* amplitude.

In summary, the NORSAR data establish that the propagation of the *Lg* phase from Novaya Zemlya to Norway is partially blocked, and that the shear

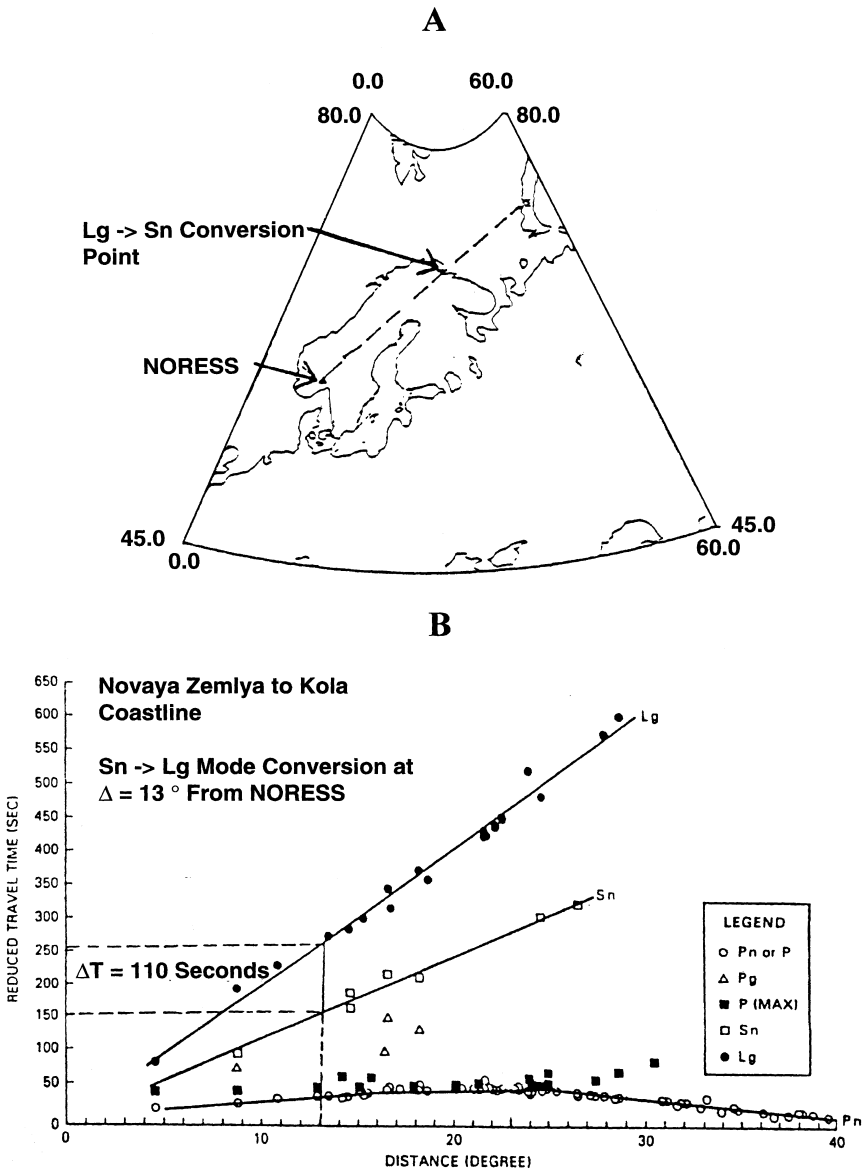

Figure 3
(A) Map showing the path from Novaya Zemlya to NORSAR. The distance from the edge of the Kola Peninsula to NORSAR is indicated. (B) Travel-time curve, after GUPTA *et al.* (1980), showing the distance and the *Sn* to *Lg* time difference of 110 seconds for a presumed *Sn*-to-*Lg* mode conversion at the coast.

phases from Novaya Zemlya are dominated by the *Sn* phase and an *Sn*-to-*Lg* mode conversion at the Barents Sea–Kola Peninsula interface. A direct *Lg* can also be inferred on the incoherent-beam traces, which is more apparent on the

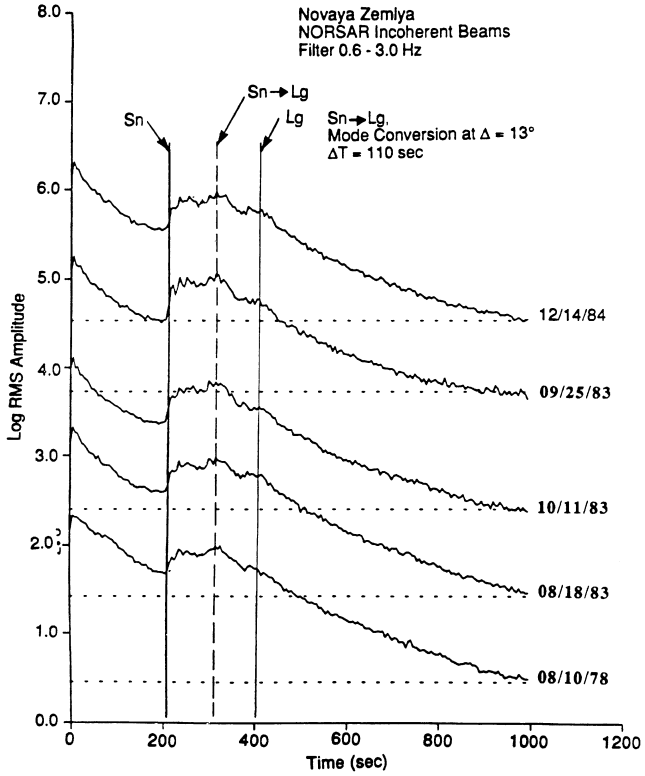

Figure 4
Incoherent beam plots at NORSAR, starting just after the maximum *Pn* amplitude, for Novaya Zemlya explosions. Plots have been shifted for display purposes. Dashed lines indicate the average noise level ahead of the *Pn* phase. The assumed times for the *Sn* and presumed *Sn*-to-*Lg* mode conversion at the Kola Peninsula coast are indicated.

NORSAR beams than on the NORESS beams studied by BAUMGARDT (1990). Although the *Sn* coda at the expected time for *Lg* does have high signal-to-noise ratio, this phase has apparently been considerably attenuated along the propagation path.

ARCESS, NORESS, and Grafenberg Array Observations

Figure 1(B) shows the propagation paths for a "reversed profile" of the one shown in Figure 1(A) that incorporates the broadband Grafenberg array and the regional arrays, NORESS and ARCESS. The event parameters of the Novaya Zemlya explosions that have occurred since ARCESS began recording data are presented in Table 2.

The vertical-component waveforms for the three explosions recorded at the ARCESS array center element (ARA0) are shown in Figure 5. The phase marked "early *Lg*" has an apparent group velocity of about 4.3 km/sec, which is considerably faster than the expected 3.5 km/sec velocity of direct *Lg*. There is virtually no energy at the 3.5 km/sec time.

The results of incoherent beam analysis for the December 4, 1988 event are shown in Figure 6 as a record section of logged rms incoherent beams for the ARCESS and

Table 2

Event parameters for Novaya Zemlya events recorded at NORESS, ARCESS, and Grafenburg

Date	Time	Latitude	Longitude	m_b
05/07/88	22:49:58.0	73.35	54.47	5.6
12/04/88	05:19:53.6	73.49	54.18	5.7
10/24/90	14:57:54.7	42.86	54.66	5.4

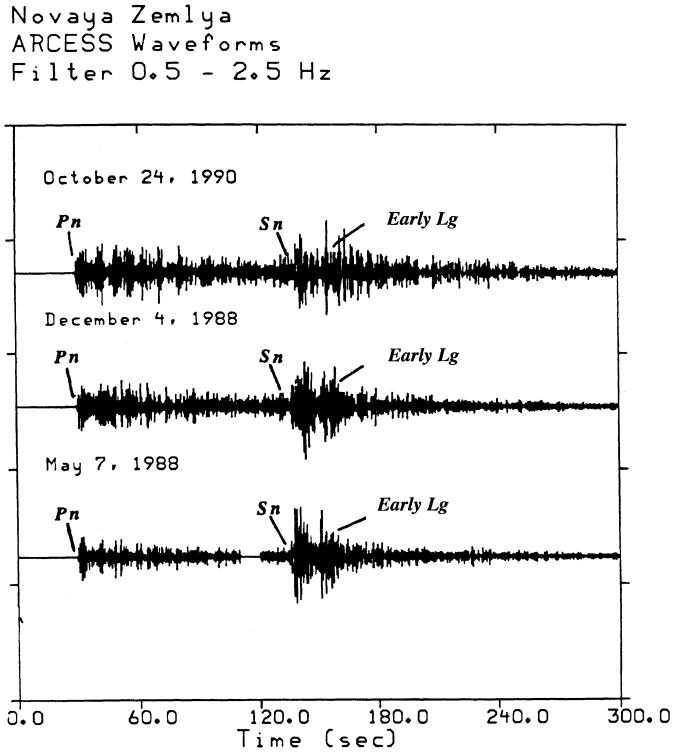

Figure 5
ARCESS recordings of recent Novaya Zemlya explosions. The times of *Pn*, *Sn*, and the inferred early *Lg* are indicated.

NORESS vertical components. The interesting features visible in the ARCESS recordings of the Novaya Zemlya explosions are that the *Sn* waves have clear onsets and amplitudes which exceed the *P* wave amplitudes, and the amplitudes increase 10 to 15 seconds into the *Sn* coda. This later coda energy is the "early *Lg*" arrival observed at NORSAR and NORESS. Since NORESS and NORSAR are collatated, the "early *Lg*" phase can be seen in the short-period data from both arrays. The relative arrival time between the secondary pulse at ARCESS and the "early *Lg*" at NORESS is consistent with an *Lg* group velocity of 3.5 km/sec.

Figure 7 shows a plot of the Grafenburg incoherent beams for the Novaya Zemlya explosions. A 0.6 to 3.0 Hz bandpass filter was applied to each waveform prior to computing the incoherent beams. The instrument response of the Grafenburg sensors, described by HARJES and SEIDL (1978), does not significantly differ from that of the Norwegian arrays in the narrow 0.6 to 3.0 Hz passband.

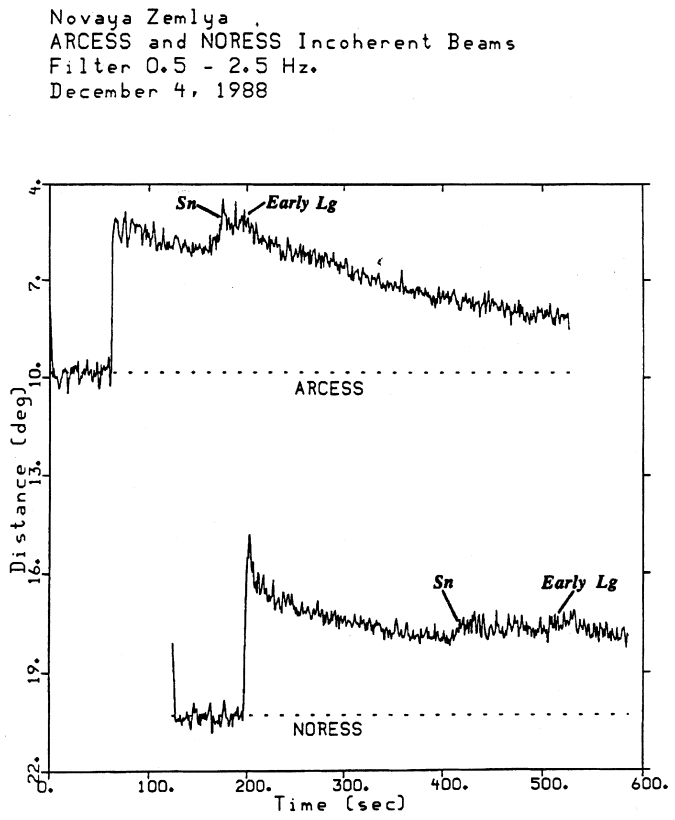

Figure 6
Record section of the incoherent beams for the December 4, 1988 Novaya Zemlya explosion recorded at ARCESS and NORESS.

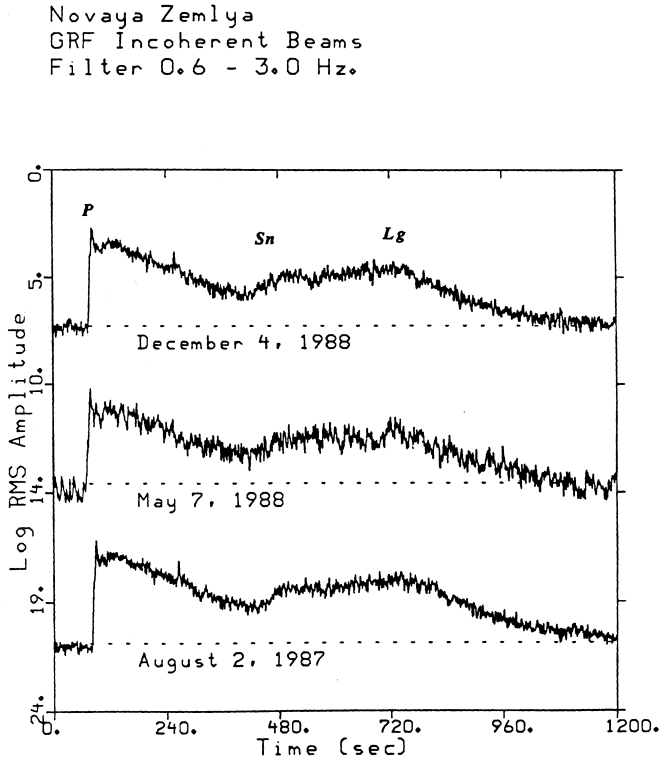

Figure 7
Incoherent beams for the Novaya Zemlya explosions recorded at the Grafenburg array.

Figure 7 shows that *Lg* is larger than *Sn* at Grafenburg for the Novaya Zemlya events, although *Lg* is emergent. The beginning of the *Sn* energy is also quite emergent with no clear onset. The *Sn* coda also appears to gradually increase with time to the peak *Lg* amplitude which indicates that the *Lg* energy may be superimposed on the scattered energy of the *Sn* coda. The expected time for the arrival of direct *Lg* for the three incoherent beams is indicated in the top plot. An *Lg* onset is most visible on the incoherent beam of the May 7, 1988 incoherent beam, whereas on the other beams the *Sn* coda appears to be continuous through the *Lg* time. Thus, although *Lg* is blocked to the Norwegian arrays such that the on-time *Lg* has energy less than the maximum *Sn* energy, more *Lg* energy does appear to get through to the Grafenburg array at approximately the time expected for direct *Lg*.

Comparison of Kola PNE (NORSAR) and Novaya Zemlya Nuclear Explosion (ARCESS)

Figure 8 compares the great-circle propagation paths for *Lg* from two different events, recorded at different times and at different arrays. The two great circle

propagation paths are a similar distance. However, the Barents Sea constitutes most of the propagation path from Novaya Zemlya to ARCESS. The path from the Kola Peninsula to NORSAR does cross the northern tip or the Gulf of Bothnia, but most of the path is continental.

Figure 9 compares the ARCESS (top) and NORSAR (bottom) waveforms for the two events in the bandpass filter from 0.6 to 3.0 Hz. This filter reduces low-frequency noise and allows comparison NORSAR and ARCESS seismograms even though they have different recording instrumentation. The ARCESS recording has no apparent *Lg* at the expected arrival time for the 3.5 km/sec *Lg*. However, a strong *Lg* was recorded from the Kola Peninsula PNE.

Geological Explanation for the Barents Sea Lg Blockage

To illustrate how these geological heterogeneities may block *Lg* propagation across the Barents Basin, crustal cross sections for the great-circle propagation paths from Novaya Zemlya to the Norwegian arrays and the Grafenburg array have been plotted in Figures 10(A), (B), and (C). These plots were produced using information available from the Cornell Geographic Information System (GIS) database for Eurasia (FIELDING *et al.*, 1992) and the Profile Maker GIS access process at the Cornell website (http://atlas.geo.cornell.edu). The top plot shows the elevations obtained for the great-circle path from Novaya Zemlya through the receiver. The topography comes from the GTOPO30 database of the EROS Data Center (EROS, 1996). The horizontal axis indicates the distance from the array along the path, with the array located on the left edge of the plot. The approximate location of the Novaya Zemlya explosion site is marked with an asterisks. The bottom plots give the inferred crustal cross section of depth to basement and Moho depth. The current database at Cornell for basement and Moho depths in Eurasia derives from

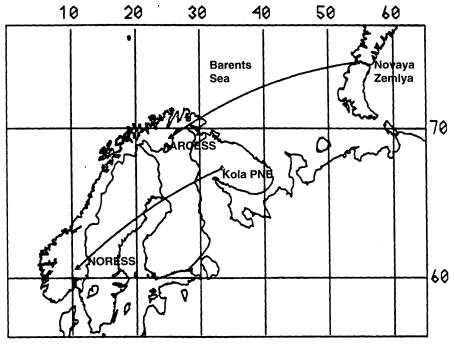

Figure 8
Map showing great-circle paths from the Novaya Zemlya test site to ARCESS and the Kola PNE to NORSAR.

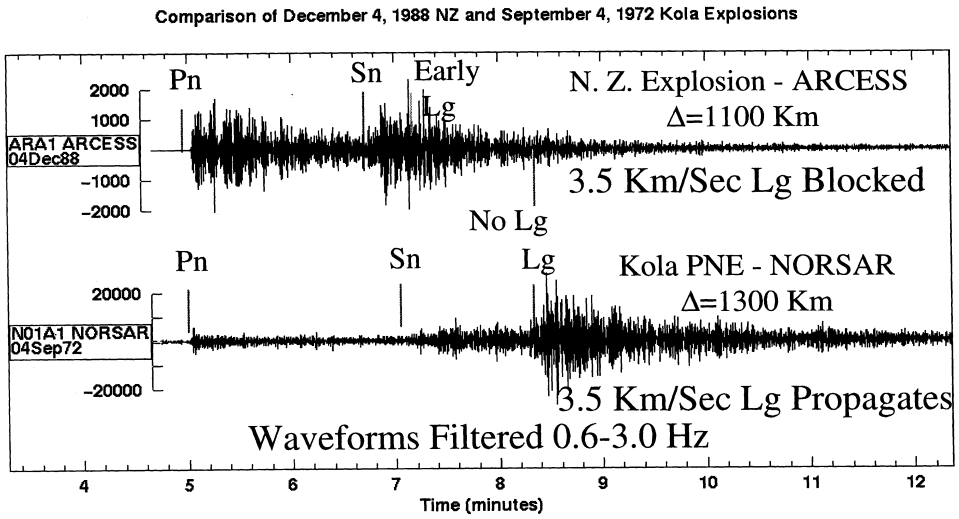

Figure 9
Comparison of the ARCESS ARA1 recording of a Novaya Zemlya explosion and the NORSAR NO1A1 recording of the Kola PNE with 0.6 to 3.0 prefilter.

digitization of maps obtained from the Institute of Physics of the Earth in Moscow, Russia (KUNIN *et al.*, 1987, 1988). The labels on the figures were obtained from tectonic maps of ALVERSON *et al.* (1967) and CLARKE and RACHLIN (1990).

In the case of the paths to ARCESS, NORESS, and Grafenburg in Figures 10(A), (B), and (C), respectively, the elevation falls quickly to the south of the Novaya Zemlya elevations, up to 6000 m, into the Barents Basin, which has a gradual slope to its deepest depth of below 300 m beneath sea level. For the path to Grafenburg in Figure 10(C), the depth and width of the Barents Sea is not quite as large as it is for the ARCESS and NORESS paths. For all three paths a very sharp increase in elevation marks the interface between the Southern Barents Basin and the Kola Peninsula.

For all three paths sediment thicknesses reaching 20 km are indicated in the same part of the structure where the Moho rises by about 5 to 10 km. This essentially reflects the general view of the basin portrayed in the Soviet geological literature, according to CLARKE and RACHLIN (1990), that the terrigenous sediments replace the granitic layer present in other parts of the path, specifically beneath Novaya Zemlya and the Kola Peninsula. Based on seismic profiles of the basin, the sediment velocities range from 3.9 to 5.5 km/sec in the sediments in contrast to the 6.0 to 6.5 km/sec velocities in the granitic layer. This would correspond to a shear-wave velocity contrast of about 2.2 to 3.17 km/sec for the sediments and 3.46 to 3.75 km/sec for the granitic rocks. This contrast in velocities would produce a strong impedance contrast at the boundaries of the basin and thus seismic energy

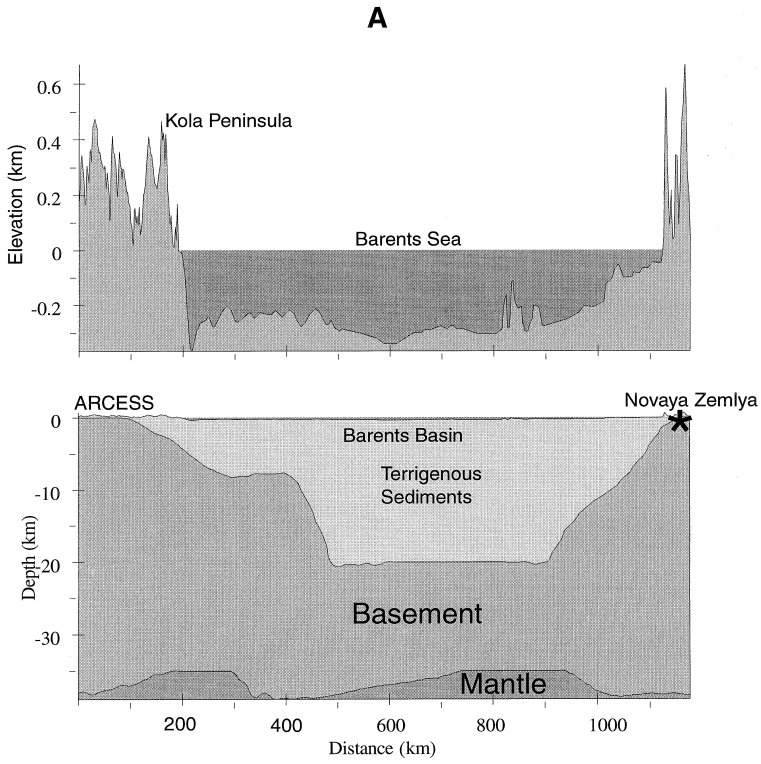

Figure 10A

that propagates into the basin may be captured and attenuated by repeated reverberations within the basin.

Figure 10(A) indicates that the distance of ARCESS from the Barents–Kola interface is about 250 km. We argued earlier that the *Sn* phase might convert to *Lg* at this interface, producing the "early *Lg*" at ARCESS. Assuming a group velocity of 4.5 km/sec for *Sn* and 3.5 km/sec for *Lg*, this would imply that the *Sn*-to-*Lg* conversion should arrive about 15 seconds after the onset of *Sn*. This is consistent with the time interval of "early *Lg*" observed at ARCESS in Figures 5 and 6. Figure 10(B) shows that the distance of this interface from NORESS is approximately 1400 km, or about 13°, which implies that the mode converted *Lg* should lag *Sn* by 110 seconds, as shown in Figure 3. This is again consistent with the observations at both NORESS and NORSAR.

The cross section from Novaya Zemlya to Grafenburg in Figure 10(C) reveals crustal thinning under the Barents Sea due to a rise in the Moho depth of about 5 km, a feature not as pronounced along the ARCESS and NORSAR paths. The rest of the path to Grafenburg crosses the elevated regions of the Kola Peninsula,

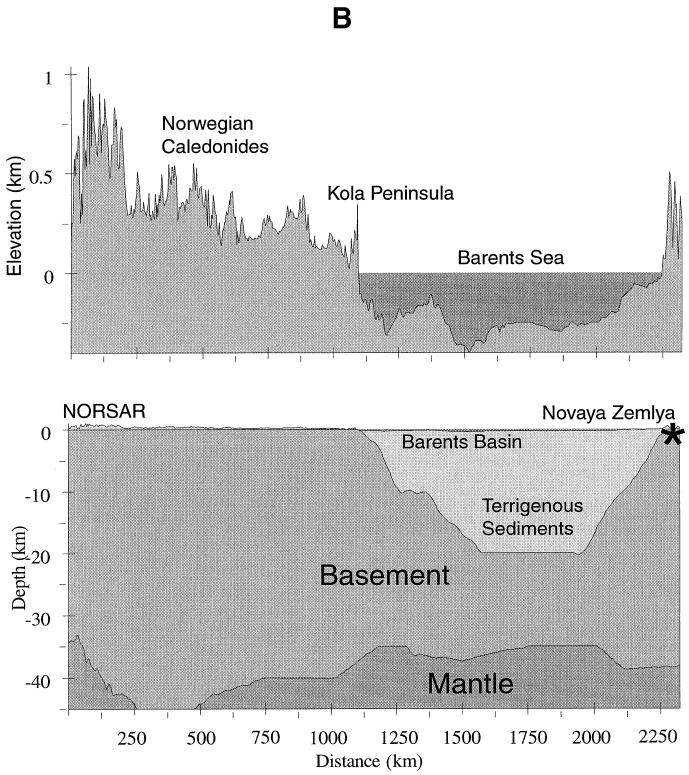

Figure 10B

Scandinavia, and the Baltic Sea, which also includes a sedimentary basin with sediment depths reaching 10 km. Moho topography varies by about ± 5 km about the average of about 35 km, although a sharp Moho dip appears at approximately 1350 km distance.

Figure 11 presents a comparison of the crustal part of the propagation paths for the two paths shown in Figure 8. The top plot shows the Barents Sea blocked-*Lg* path, with the associated sedimentary basin with sediment depths of some 20 km, and the bottom plot shows the unblocked-*Lg* path. Obviously, the sedimentary basin is the main feature of the crust that differs between these two paths and would appear to be the primary cause of *Lg* blockage across the Barents Sea.

It has been proposed that *Lg* blockage may be caused by high anelastic attenuation of *Lg* in basins with low-*Q* sediments (MITCHELL and HWANG, 1987). To check this possibility, *Lg Q* cross sections, obtained from the database of MITCHELL *et al.* (1997), are plotted in Figure 12. These *Q* values, derived by the coda method, stem from tomographic analysis of many paths in Eurasia, and the two cross sections in Figure 12 for blocked (top) and unblocked (bottom) paths were taken from the

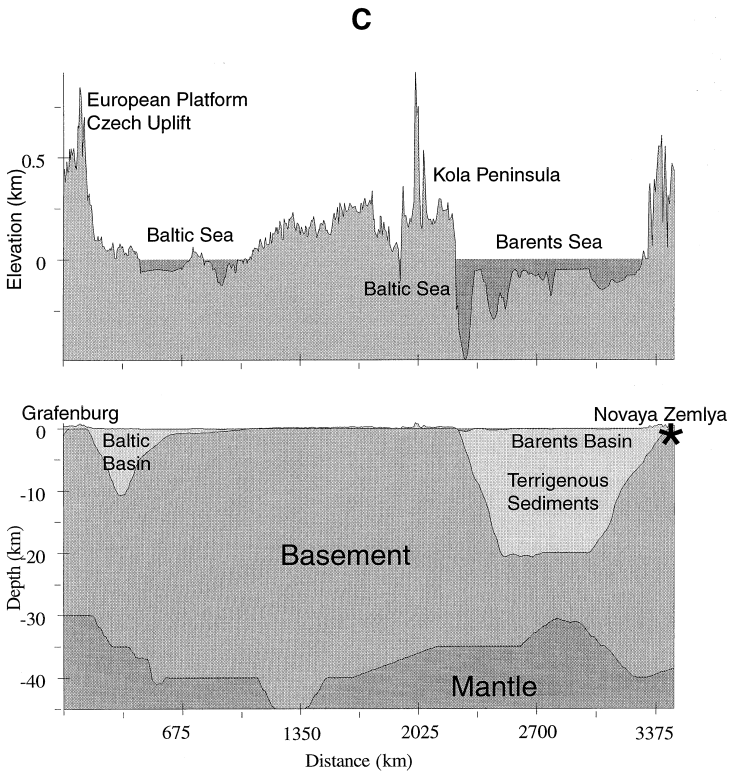

Figure 10
(A) Geological cross sections of the propagation path from Novaya Zemlya ARCESS. Top plot is a cross section of topography on an expanded vertical scale, and the bottom plot indicates the elevation, depth to basement, and depth to Moho on the same vertical scale, inferred from the Cornell Website server Profile Maker. (B) Crustal cross section from Novaya Zemlya to NORSAR. (C) Crustal cross section from Novaya Zemlya to the Grafenberg Array.

tomographic images. Both plots show that the average Q in both regions is high, with averages of 917 and 875 for the blocked and unblocked paths, respectively. Thus the data set does not reveal low Q in the Barents Sea Basin. However we cannot rule it out because the tomographic maps may not be accurate for this region, since the Barents Sea is near the edge of the overall Eurasian map region and the values in this region may reflect extrapolation.

Based on this analysis of crustal cross sections for the *Lg* propagation paths from Novaya Zemlya to the ARCESS, NORESS, and Grafenburg arrays, we conclude that the main cause of the *Lg* blockage in the Barents Sea, for the paths to the Norwegian stations, is the presence of thick sediment accumulations in the sedimentary basin beneath the southern part of the Barents Sea. Moho depth variations do not appear to be significant over most of these paths. Elevation changes are quite sharp but are actually quite small when compared to the overall thickness of

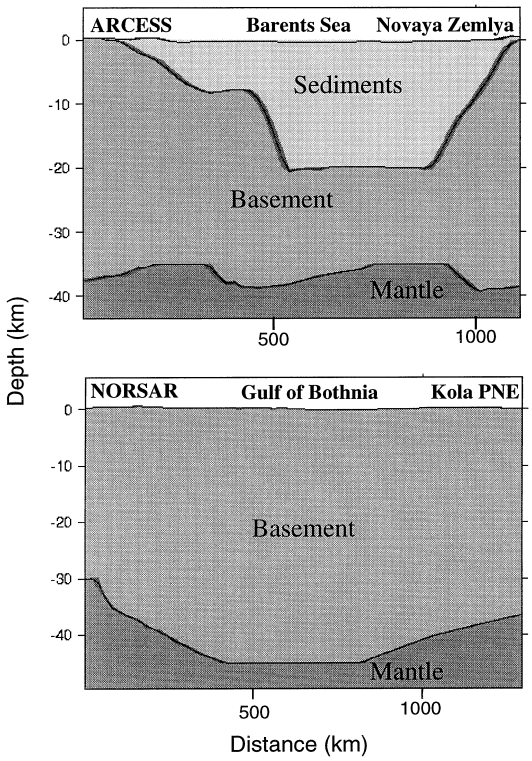

Figure 11
Comparison of crustal cross sections from Novaya Zemlya to ARCESS (top) and from the Kola PNE to NORSAR (bottom).

the crust. The same can be said for the presence of water in the basins, which is only a few hundred meters on average. Since the wavelength of *Lg* is on the order of a few kilometers at frequencies near 1 Hz, the variation in elevation and water depth is decidedly less than a wavelength. Since sediment depth variations are on the order of several wavelengths, this would appear to be a more likely cause of *Lg* blockage in this region.

Lg is better observed at Grafenburg than at either ARCESS and NORESS, in spite of the considerably longer propagation path to Grafenburg. Moreover, the Grafenburg incoherent beams contain significant energy in the codas of both *P* and *Sn*. These coda waves may be generated by scattering of the crustal guided phases, primarily *Sn* and *Lg*, from the geological and topographic heterogeneities along the path. For example, Figure 10(C) displays several topographic and geologic heterogeneities along the propagation path from Novaya Zemlya to the Grafenburg array that may be scattering sources, including the Kola Peninsula, the Barents and Baltic Basins, and the contacts between the Barents Basin and Kola Peninsula and between the Baltic Basin and European Platform and Czech Uplift. Both shear modes, *Sn* and

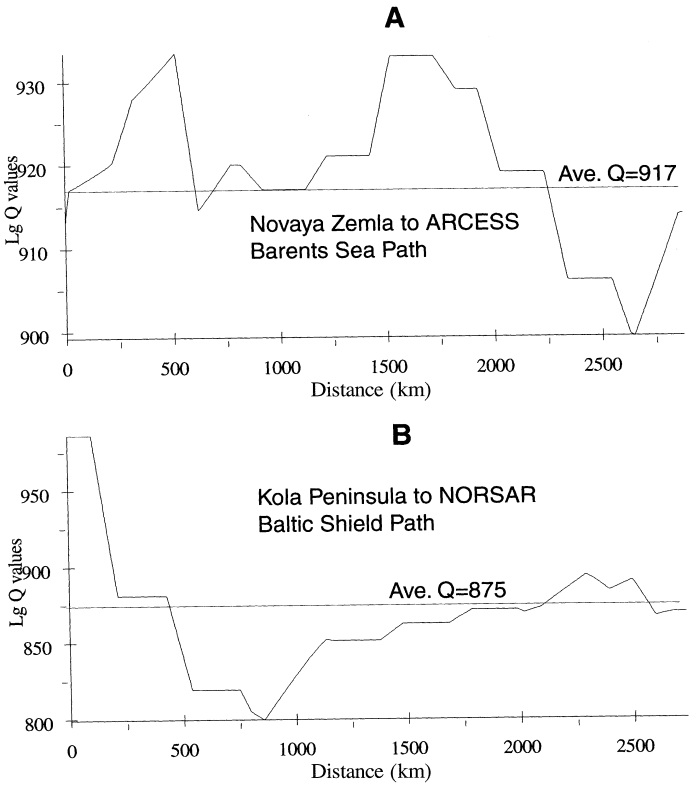

Figure 12
Cross sections through the *Lg Q* tomographic map for Eurasia (MITCHELL *et al.*, 1997). (A) Barents Sea path. (B) Baltic Shield path.

Lg, can interconvert to each other as well as forward scatter into *Pn* and *P* modes, thus building up the pre-*Sn* coda. Figure 7 shows that the *Sn* coda builds up after the onset of *Sn* and that "early *Lg*" energy may be produced by cumulative scattering from the heterogeneities along the propagation path.

Southern Urals and Caspian Sea Basins

We now consider the long-range ($\Delta > 2000$ km) propagation of *Lg* across sedimentary basins in Eurasia to NORSAR. An earlier study (BAUMGARDT, 1985) has revealed partial blockage of *Lg* across the Ural mountains, although the precise cause of the blockage was considered to be scattering of *Lg* in the crust beneath the Urals. Moreover, *Lg* has been known for some time to propagate inefficiently across the Caspian Sea region (e.g., KADINSKY-CADE *et al.*, 1981; PIWINSKII, 1981;

RODGERS *et al.*, 1997). Two sets of data have been examined that probe this region. First, historical PNEs in the FSU, recorded at the NORSAR array, have been studied with paths that cross the Southern Urals and the northern part of the Caspian Sea. Second, a new data set of seismic events recorded at the Iranian Long Period Array (ILPA) has paths that cross the southern part of the Caspian Sea.

NORSAR Observations – Southern Urals and Northern Caspian Sea

Figure 13 shows the great circle paths from four PNEs on either side of the Ural Mountains and the Northern Caspian region to NORSAR. The source parameters of the events are listed in Table 3. The two Southern Urals PNEs, 10/22/71 and 11/24/72, occurred on opposite sides of the Ural Mountains. The Astrakhan event of 10/08/80 and the East Caspian Sea event off 12/23/70 occurred on opposite sides of the Northern Caspian Sea. The paths from these events to NORSAR cross over several

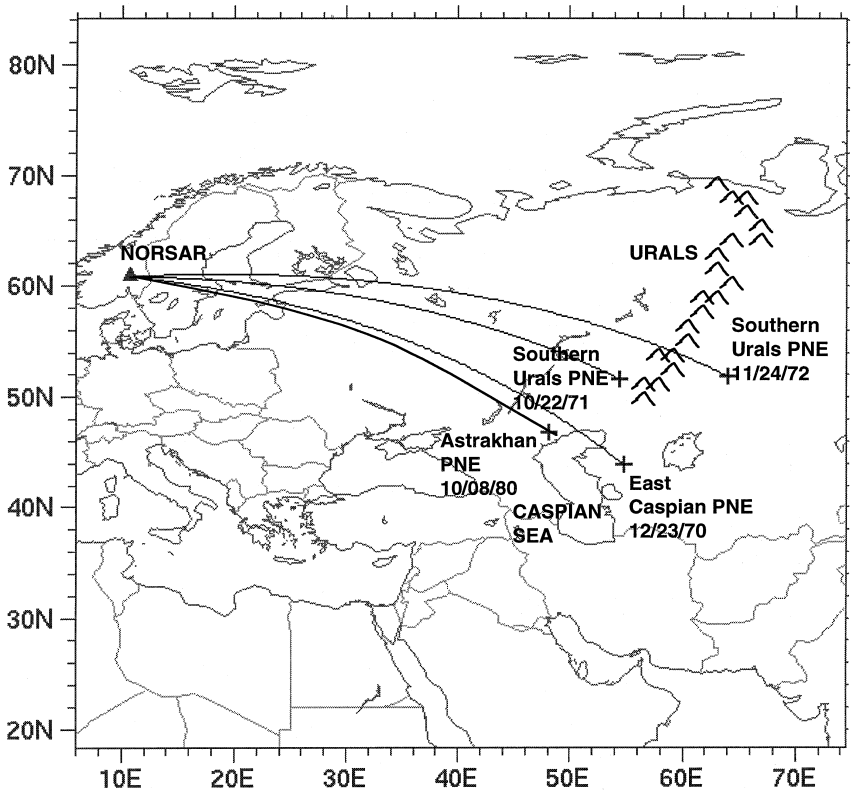

Figure 13
Great circle paths to NORSAR from PNEs in the southern Ural Mountains, Astrakhan, and east of the Caspian Sea.

Table 3

Event parameters for PNEs near Northern Caspian Sea recorded at NORSAR

Date	Time	Latitude	Longitude	m_b	Region
12/23/70	07:00:57.3	48.83	54.85	6.6	East of Caspian Sea
10/22/71	05:00:00.0	51.56	54.53	5.2	Southern Urals
11/24/72	09:59:57.8	54.84	64.15	5.2	Southern Urals
10/08/80	06:00:00.0	46.70	48.21	5.2	Astrakhan

heterogeneous structures in the source region but share common paths nearer the receiver.

The incoherent beam at NORSAR starts five seconds after the *P* onset time, as described by BAUMGARDT (1985). The reason for this is that these events occur at the epicentral distance, 25 to 31°, where upper mantle triplications can significantly affect the *P*-wave amplitudes, and the relative amplitudes of *P* and *Lg* may relate more to upper mantle effects on *P* rather than to crustal structure effects on *Lg*. In order to focus more on possible blockages of *Lg*, the *P* amplitude variations are ignored by starting the windows five seconds into the coda and comparing the *Lg* amplitudes with *P*-coda levels.

Furthermore, as was done in the earlier study of BAUMGARDT (1985), the coda incoherent beam envelopes were computed from the smaller NORSAR array configuration that was set up after 1 October 1976. This then ensures that the same sensors were used in the analysis of the events before and after 1976. The windows used to calculate the incoherent beams begin 5 seconds after the *P*-onset time on each trace. These times were measured by hand with an accuracy of about 0.3 to 0.5 seconds. Thus, these beams have, in affect, been "steered" to the velocity and azimuth of the *P* wave. Only the vertical component waveforms were used in computing the envelopes, and the waveforms were all bandpass-filtered from 0.6 to 3.0 Hz prior to calculating the beams. The average noise levels in the prior 50 seconds of noise were also computed and plotted as horizontal lines on the incoherent beam plots.

Figure 14(A) compares the NORSAR incoherent beams for the 10/22/71 Southern Urals event and the 10/08/80 Astrakhan event. The two events have the same magnitudes ($m_b = 5.2$) and epicentral distances (about 26°) from NORSAR. The beams are plotted on the same absolute amplitude scale, with log-rms amplitude units, and the horizontal line indicates the average noise level for both events. The early *P*-coda levels and the secondary *PP* phase nearly overlap with the same amplitude. The phase labeled *PP* may also consist of other long-range coda phases, such as $P_{410}P$ and "whispering gallery" phases (*WG* and WG_{fs}), that have been identified by MOROZOVA *et al.* (1998) on long-range Quartz profiles across the Urals, and correspond to the large-distance propagation of the *Pn* phase. However,

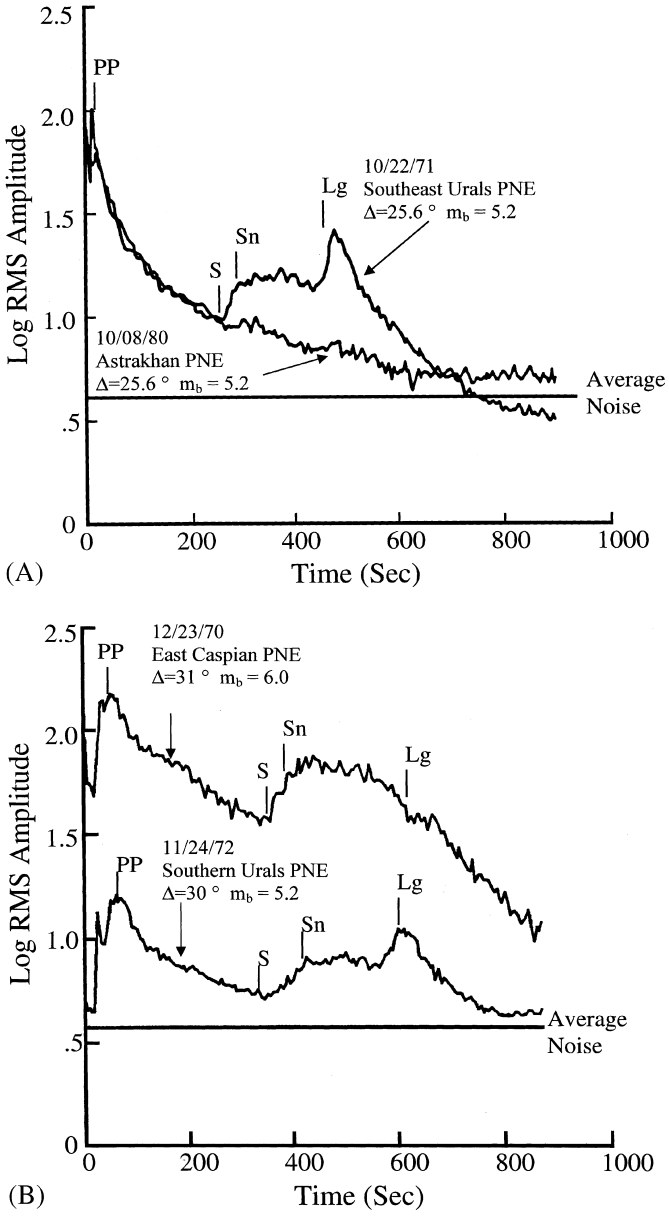

Figure 14
(A) NORSAR incoherent beams of the Astrakhan PNE and the Southern Urals PNE, located west of the Urals, beginning just after the peak *P* amplitude. (B) Comparison of NORSAR incoherent beams from the East Caspian PNE and the Southern Urals PNE located east of the Urals.

beginning at the *S* onset time, the beams are very different. The Southern Urals event has a very strong *Sn* and *Lg* phase whereas these phases are absent for the Astrakhan event.

Figure 14(B) compares the 11/24/72 Southern Urals event with the East Caspian PNE of 12/23/79. These events are also about the same distance, 30° and 31°, however the magnitudes are very different which is why the East Caspian PNE, with $m_b = 6.6$, has a much higher amplitude in the entire coda than the Southern Urals PNE, with $m_b = 5.2$. Aside from the amplitude differences, the codas of these two events have similar features and decay slope from *PP* to the expected *S*-arrival time. However, the East Caspian PNE does not have a strong direct *Lg* whereas the 11/24/72 Southern Urals PNE has an *Lg* that is larger than the *S* and *Sn* phases.

Thus, these comparisons suggest that *Lg* may be blocked from the Astrakhan and East Caspian events, both located in the Northern Caspian region, although *Lg* propagates efficiently from the two Southern Urals PNEs at comparable distance. Also, *Sn* is missing for the Astrakhan event but propagates efficiently from the other events to NORSAR. Figure 13 illustrates that the two Southern Urals PNEs occurred on opposite sides of the Urals relative to NORSAR. However, *Lg* does not appear to be blocked from the 11/24/72 event whose *Lg* propagation path crosses the Urals. Both events had equally strong *Lg* with amplitudes greater than the preceding *S* and *Sn* phases.

The South Ural and Pri-Caspian Sedimentary Basin Structures and Lg Blockage

To search for possible causes of the various blockages, we compare the four crustal cross sections for these events, plotted in Figures 15(A), (B), (C), and (D), that were derived from the Cornell Eurasia elevation, basement-depth, and Moho-depth databases using Profile Maker, as discussed earlier. The region northwest of the Caspian Sea includes a large sedimentary basin called the Pri-Caspian (PIWINSKII, 1981) that appears in the cross sections for the Astrakhan and East Caspian events in Figures 15(B) and 15(D), respectively. This basin is similar to the Barents Basin in that the post-Paleozoic sediments reach extraordinary depths in excess of 20 km. Also, the basin contains extensive evaporite deposits in the form of salt domes that are exposed at the surface. The East Caspian event occurred on the extreme east end of the basin and thus *Lg* would propagate across this very deep basin before entering the Voronezh Uplift on the Russian Plateau. The Astrakhan event occurred in the basin, north of the Caspian Sea, and the *Lg* propagation path did not cross the water segment. This indicates that the North Caspian or Pri-Caspian Depression, not the shallow Caspian Sea itself, blocks the *Lg* propagation across the region.

The missing *Sn* as well as *Lg* in the case of the Astrakhan explosion may not be entirely explainable as a blockage effect. Astrakhan explosions are known to have been detonated in salt (MURPHY *et al.*, 1997), and the salt source medium may be fairly homogeneous. Thus, these detonations in salt may not have excited strong

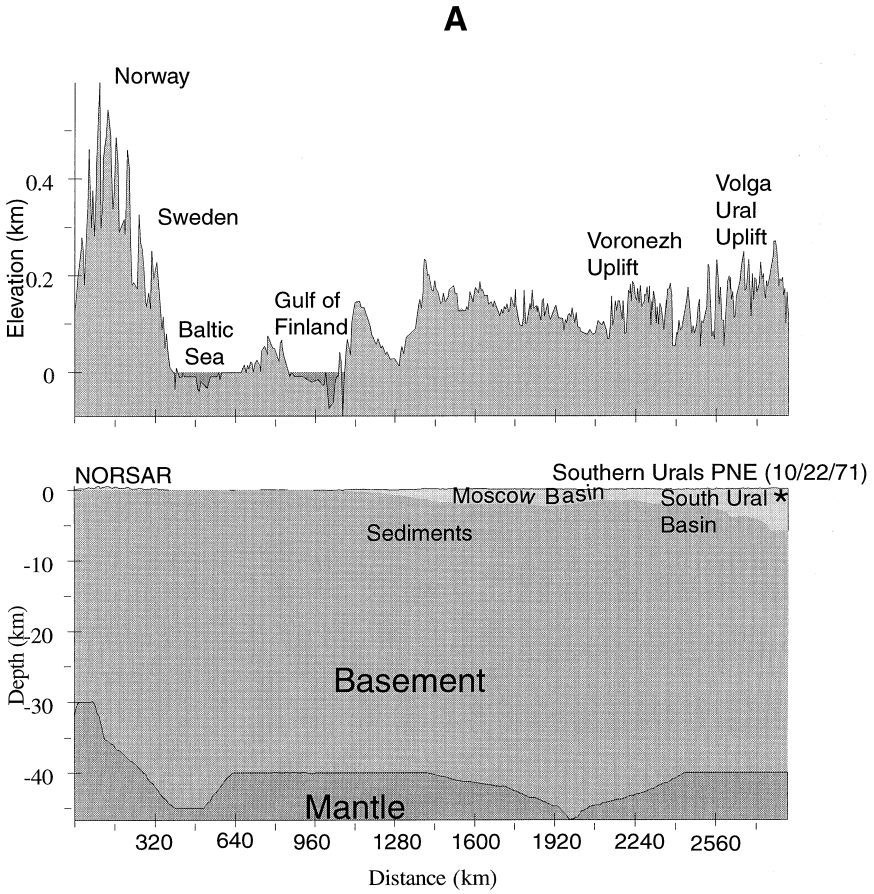

Figure 15A

shear waves. MURPHY *et al.* (1997) also reported low *Sn* amplitudes relative to *Pn* for Astrakhan explosions recorded at the Russian station at Borovoye.

The two Southern Urals PNEs were also detonated in a sedimentary basin called the South Ural Basin, which is evident in the crustal cross sections in Figures 15(A) and (C). However, this basin does not block the *Lg*, and in fact, *Lg* is strongly excited from both these sources. One possible explanation for why *Lg* is not blocked here, and is blocked by the Caspian Basin, may relate to where the PNE occurs relative to the basin, the depth of sediments and width of the basin. If the event occurs outside the basin and *Lg* must cross the entire basin, as in the case of the two Caspian events, there may be more *Lg* blockage than if the event occurs in the basin itself.

The Caspian Basin is considerably larger, both in width and depth of sediments, than the Southern Urals Basin. Also, in the case of the Caspian Basin, there is a sharp topographic interface between the basin and the adjacent Voronezh Uplift,

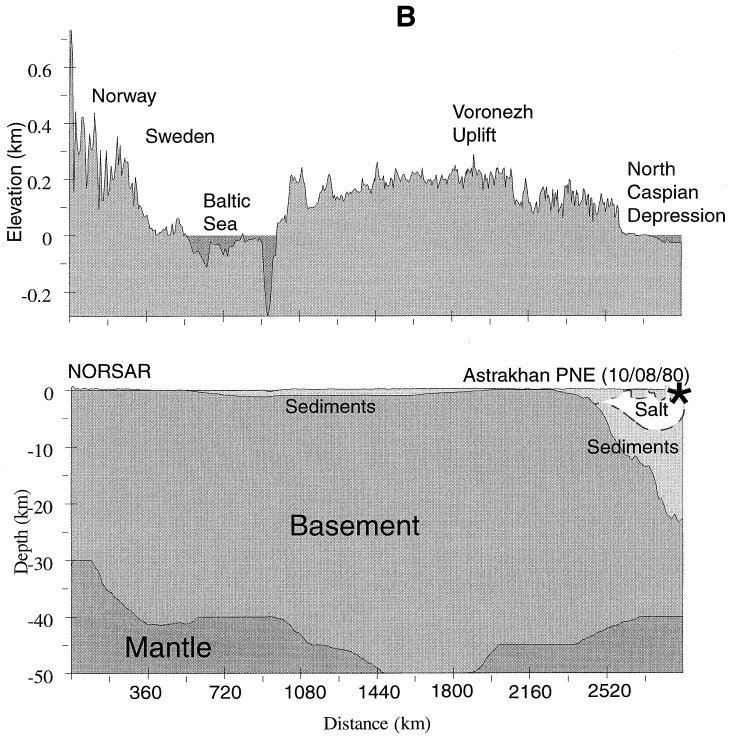

Figure 15B

similar to the Barents Sea–Kola interface, which may significantly backscatter *Lg* waves. This interface could also be a source of *Sn*-to-*Lg* scattering that produces the complex *Sn* coda observed from the East Caspian event. The "bumps" in the *Sn* coda in Figure 14(B) may actually be "early *Lg*" waves produced by this conversion. As regards the Southern Urals PNE located to the west of the Urals, shown in Figure 15(A), the South Ural Basin actually underlies an elevated region and there is no sharp vertical interface between the Volga-Ural Uplift and the edge of the basin that could backscatter *Lg*. However, Figure 15(C) illustrates that the path from the 11/24/72 Southern Urals PNE must cross both the South Ural Basin and the Moscow Basin as well as the Ural Mountains and yet none of these features appear to block *Lg* propagation from this event.

Thus we are left with the question of why the Pri-Caspian Basin blocks *Lg* propagation whereas the South Urals Basin does not? As discussed above, the difference in size and depth of sediments in the two basins, with the Pri-Caspian Basin being substantially larger with thicker sediments than the South Ural Basin, may be part of the explanation. Another may be that the sediments in the Pri-Caspian Basin have lower Q than those in the South Ural Basin. To check this possibility we examine *Lg* Q cross sections for the four paths, taken from the

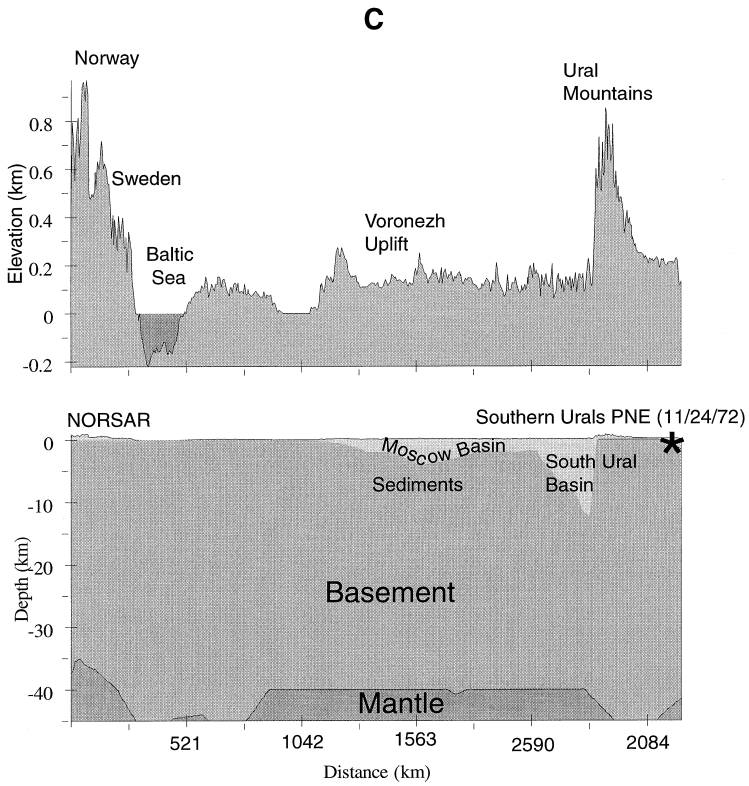

Figure 15C

Eurasian *Lg Q* tomographic map of MITCHELL *et al.* (1997). Figures 16(A) and (B) show the *Lg Q* cross sections for the Southern Urals PNEs and Figures (C) and D show the values for the Astrakhan and East Caspian PNEs, respectively. *Lg Q* does decrease along the path from NORSAR to both basins, although the drop in *Lg Q* is far greater for the Caspian paths than for the Urals paths. The average *Q* is the Pri-Caspian Basin is less than 400, significantly less than the average value of about 700 in the South Ural Basin. Consequently the combination of the low *Lg Q* as well as differences in morphology of the basins might explain why the Pri-Caspian Basin blocks *Lg* although the South Urals Basin does not.

Iranian Long-period Array (ILPA) Observations – Central and Southern Caspian Sea

We now consider *Lg* propagation across the central and southern parts of the Caspian Sea region using a new data set that has recently been made available, consisting of seismic events in the Southern Caspian Sea region recorded at the

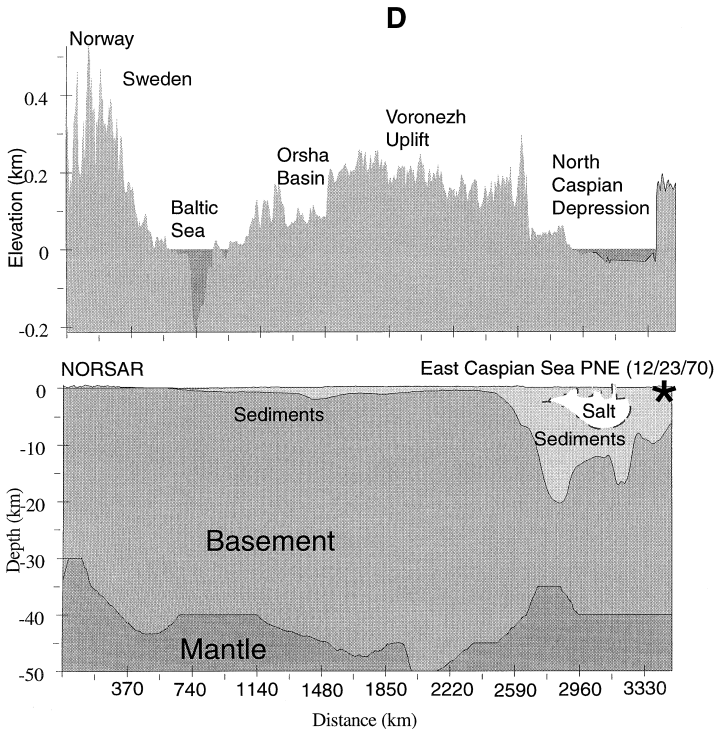

Figure 15
Crustal cross sections from NORSAR to (A) 10/22/71 Southern Urals PNE, (B) Astrakhan PNE, (C) 11/24/72 Southern URALS PNE, and (D) East Caspian PNE.

Iranian Long-period Array (ILPA) (GRANT *et al.*, 1996). The event parameters are given in Table 4. The body-wave magnitudes of the events range from 4.0 to 6.0. Many of the events have determined depths that range from very shallow to subcrustal (greater than 40 km). One event, on 08/13/78, has an estimated depth of 127.9 km which is in the mantle. Note that most of events have reported depths of 33 km, which is the NEIC constrained depth when depth cannot be determined.

The KS36000 seismometers of ILPA were primarily designed for long-period seismic recording. However, ILPA also recorded in the short-period band to 10 Hz Nyquist (TEXAS INSTRUMENTS, 1977). This region was previously studied by SIKHARULIDZHE (1964), as reported by SHISHKEVISH (1979), who observed no propagation of *Lg* for paths to Russian stations across the central and southern parts of this region. RODGERS *et al.* (1997) has also studied this ILPA data set, along with other data, and reported *Lg* blockage in the Caspian Sea and other regions of the Middle East. KADINSKY-CADE *et al.* (1981) and RODGERS *et al.* (1997) attribute *Lg* blockage in this region to the presence of deep oceanic crust.

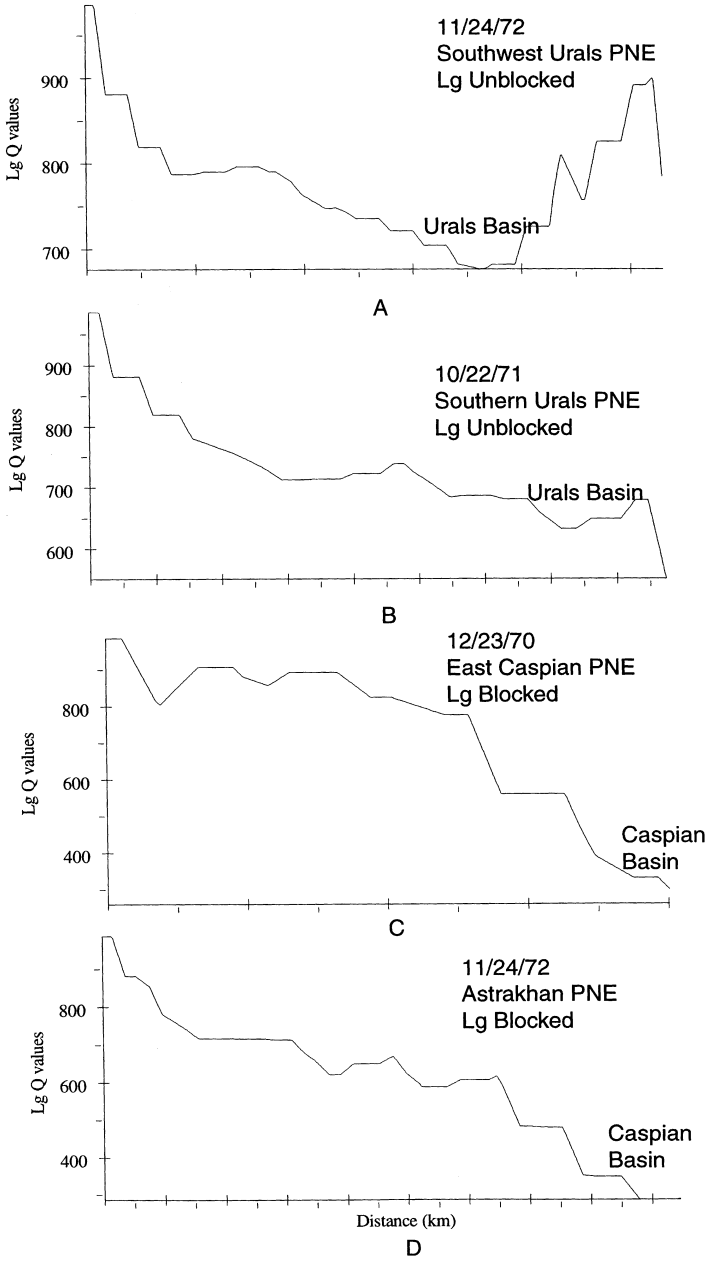

Figure 16
Lg Q cross sections to NORSAR from (A) 11/24/72 Southern Urals PNE, (B) 10/22/71 Southern Urals PNE, (C) East Caspian PNE, and (D) Astrakhan PNE.

Table 4

NEIS event parameters for events near the Southern Caspian Sea recorded at ILPA

Date	Time	Latitude	Longitude	Depth	m_b
07/20/78	10:20:25	38.664	55.243	33	4.3
07/31/78	16:37:15	40.371	52.914	33	4.3
08/13/78	17:20:25	39.328	41.072	127.9	4.3
08/15/78	09:04:22	41.249	43.989	7.8	4.7
08/20/78	02:30:03	42.292	49.982	33	4.0
08/22/78	22:48:11	41.936	43.87	3.9	4.8
08/26/78	13:10:18	36.898	54.333	33	–
08/29/78	00:19:17	41.231	49.526	0	4.4
09/03/78	00:21:17	44.451	38.012	33	5.7
09/07/78	09:19:52	38.058	58.571	33	–
09/21/78	11:08:49	38.062	38.645	30.6	4.6
10/17/78	16:45:14	39.675	41.735	33	–
11/03/78	18:54:07	42.501	45.259	33	4.4
11/04/78	15:22:20	37.713	48.946	36.8	6.0
11/16/78	05:46:09	43.499	46.623	33	3.9
11/23/78	15:24:39	44.171	39.337	25.4	4.4
11/25/78	08:57:25	39.901	44.069	10	4.4
12/04/78	03:12:38	38.068	37.43	37.3	5.0
12/14/78	05:08:23	45.494	37.36	10	4.7
12/18/78	07:59:56	47.783	48.136	33	5.9
01/01/79	04:25:39	37.638	50.176	33	4.0
05/12/79	16:19:55	41.419	48.155	33	4.2
06/08/79	17:46:10	37.074	55.616	3	4.4
06/15/79	21:15:04	36.117	54.521	33	–
08/02/79	22:42:10	40.727	52.016	67.7	4.3

Figure 17(A) shows locations of seismic events with *Lg* propagation paths to ILPA that cross the central and southern Caspian Basin. A record section of vertical component waveforms from the first ILPA channel (IR1) is plotted in Figure 18(A). The 18 December 1978 event, at a distance near 1400 km, is a nuclear explosion in the Azgir region north of the Caspian Sea. The other events appear to be earthquakes because they are located in the Caspian Sea and generally have larger *Sn* waves than *Pn* waves.

The waveforms in Figure 18(A) contain *Pn* and *Sn* arrivals. The dashed line indicates the expected arrival time of the *Lg*, however no clear arrivals are apparent at the indicated time of *Lg*. For these paths, *Lg* propagation has been blocked.

Figure 17(B) shows paths for other events recorded at ILPA, but which do not cross the Caspian Sea. Figure 18(B) shows the record section of the ILPA (IR1) recordings of these events. These waveforms are distinctly different than those in Figure 18(A) in that they contain significant energy at the expected arrival time of *Lg*. Also, these events produced considerably stronger *Pg* and coda waves than the events in Figure 18(A). The greater complexity of these waveforms may be due to the

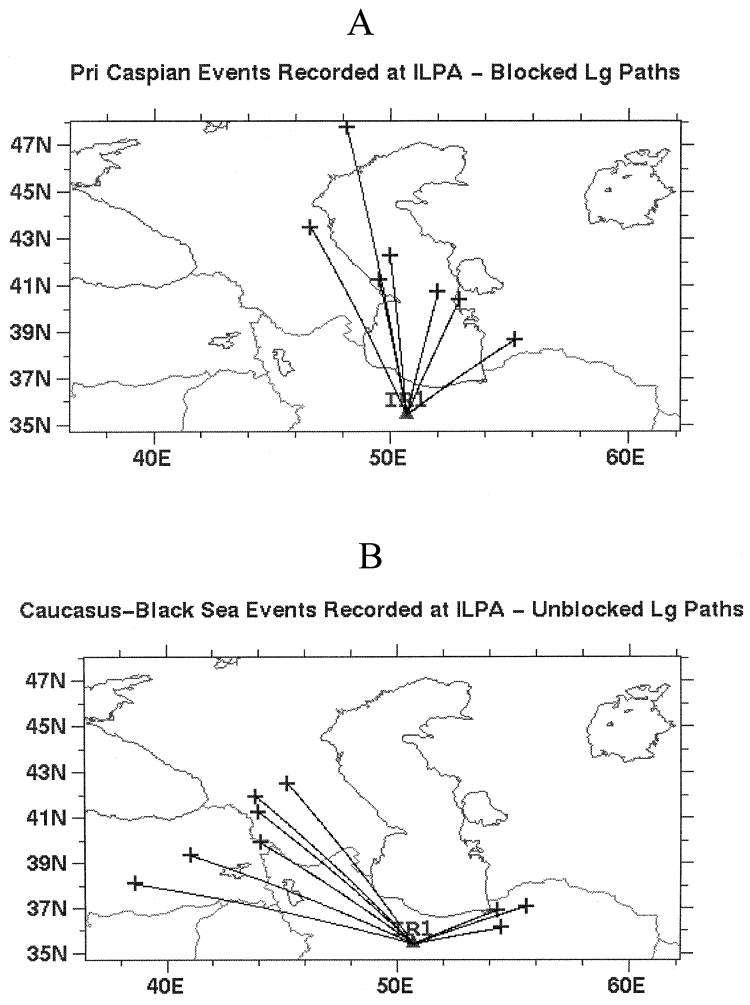

Figure 17
(A) Map showing great-circle paths from earthquakes to the ILPA array that appear to have *Lg* blockage. (B) Map showing great-circle paths from earthquakes to the ILPA array where *Lg* is not blocked.

increased complexity of the propagation paths, since many of the paths cross the Caucasus and the thrust belts of northern Iran.

Variations in source parameters, especially magnitude and depth, must also be considered as a possible cause of *Lg* amplitude variations. A detailed systematic study of possible effects of source parameters on *Lg* amplitudes has not yet been carried out. However, a cursory examination of Table 4 does not reveal strong evidence that extreme values of source parameters are a major cause of the lack of *Lg* for the events in Figure 18(A). For example, deeper events might be expected to

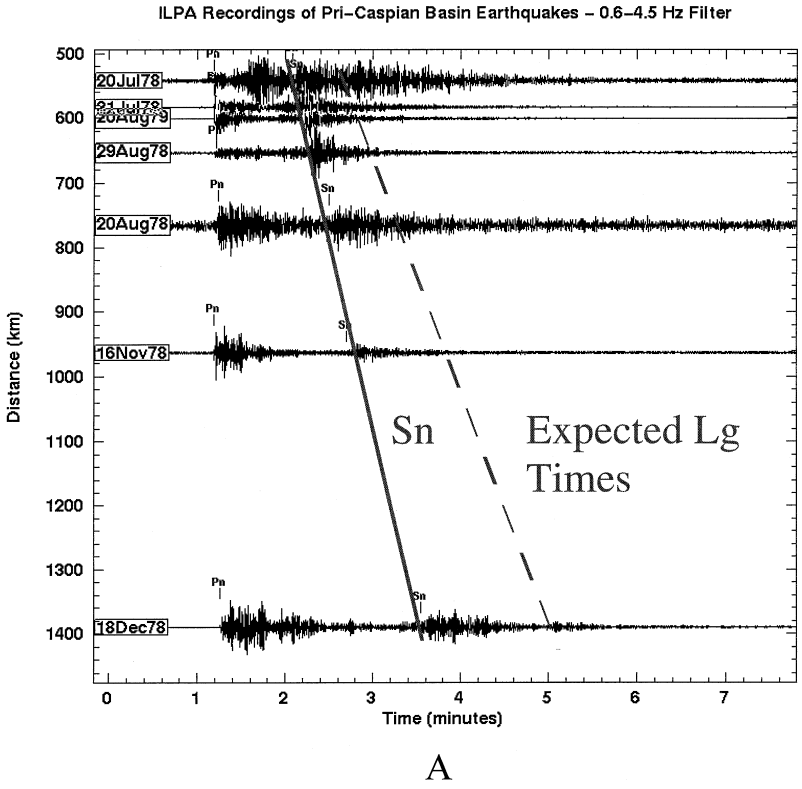

Figure 18A

underexcite *Lg* whereas shallower events would produce larger *Lg* amplitudes. The subcrustal event of 8/20/79, with depth of 67.7 km, does fall in the "blocked *Lg*" group in Figure 18(A). However, the 8/13/78 event with the mantle depth of 127.9 km produced a large *Lg* arrival in Figure 18(B), although admittedly in a very complex *P* coda. Moreover, the 8/29/78 event had the shallowest reported depth, 0 km, yet produced no *Lg*, as shown in Figure 8(A), but did produce a very large *Sn*.

South Caspian Sedimentary Basin Structure and Lg Blockage

Figure 19 gives a comparative analysis of waveforms and crustal structure for two selected paths that had blocked and unblocked *Lg*. The locations of the events and their great-circle paths to ILPA are shown in the map in Figure 19(A); their crustal cross sections are shown in (B), and (C) compares the waveforms of the two events. The West Caspian earthquake (16 November, 1978) is the event with the blocked *Lg*, and the South Caucasus earthquake (22 August, 1978) produced a strong *Lg*. Note that the blocked path from the West Caspian earthquake just skirts

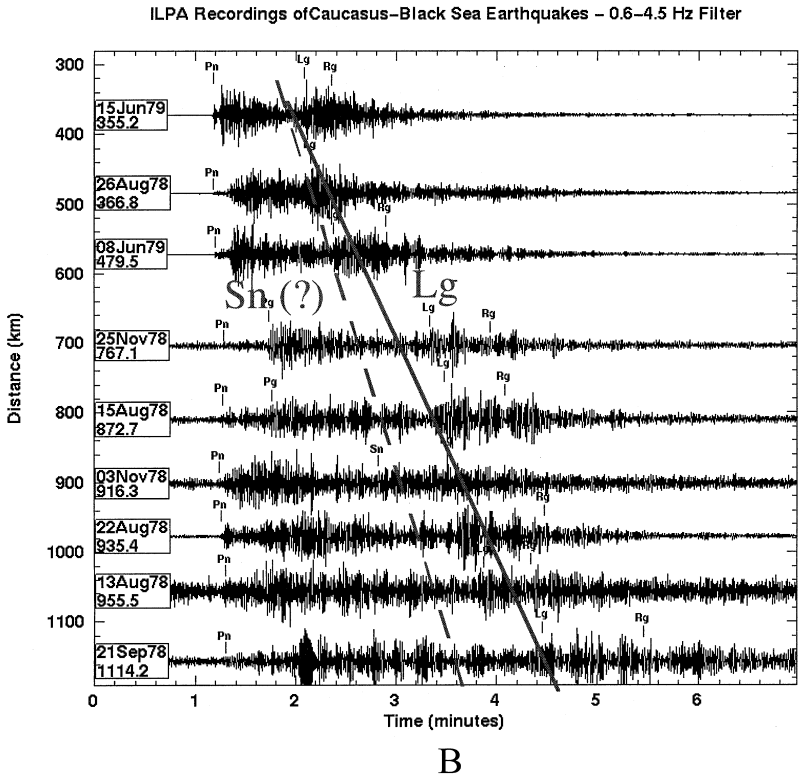

Figure 18
(A) Record section, aligned to *Pn* and corresponding to the paths in Figure 17(A), of waveforms recorded at the ILPA IR1 sensor where *Lg* arrivals phases appear to have been blocked. (B) Record section, aligned to *Pn* and corresponding to the events in Figure 13(B), of waveforms recorded at IR1 where *Lg* phases are observed.

the western edge of the southern Caspian Basin that is an enclosed sedimentary basin, with sediments reaching 12-km thickness in this region. The unblocked path misses the sedimentary basin.

The crustal structure of the deep sedimentary basins in the Caspian has been explained as a remnant of a vastly larger marginal sea that was buried during the Mesozoic collision of the Arabian promontory and the Eurasian margin (e.g., ZONENSHAIN and LE PICHON, 1986). As revealed by Russian DSS studies, the sediments in the basins have low velocity (about 3.5 km/sec) which overlie the basement rocks of considerably higher velocity (6.5 km/sec), the latter associated with the oceanic crust of the buried (Tethys) ocean. The basement rocks on either side of the basin appear to have normal granitic velocities (6.0 km/sec) (BERBERIAN, 1983). This interpretation is shown in the top cross section for the blocked path in Figure 19(B).

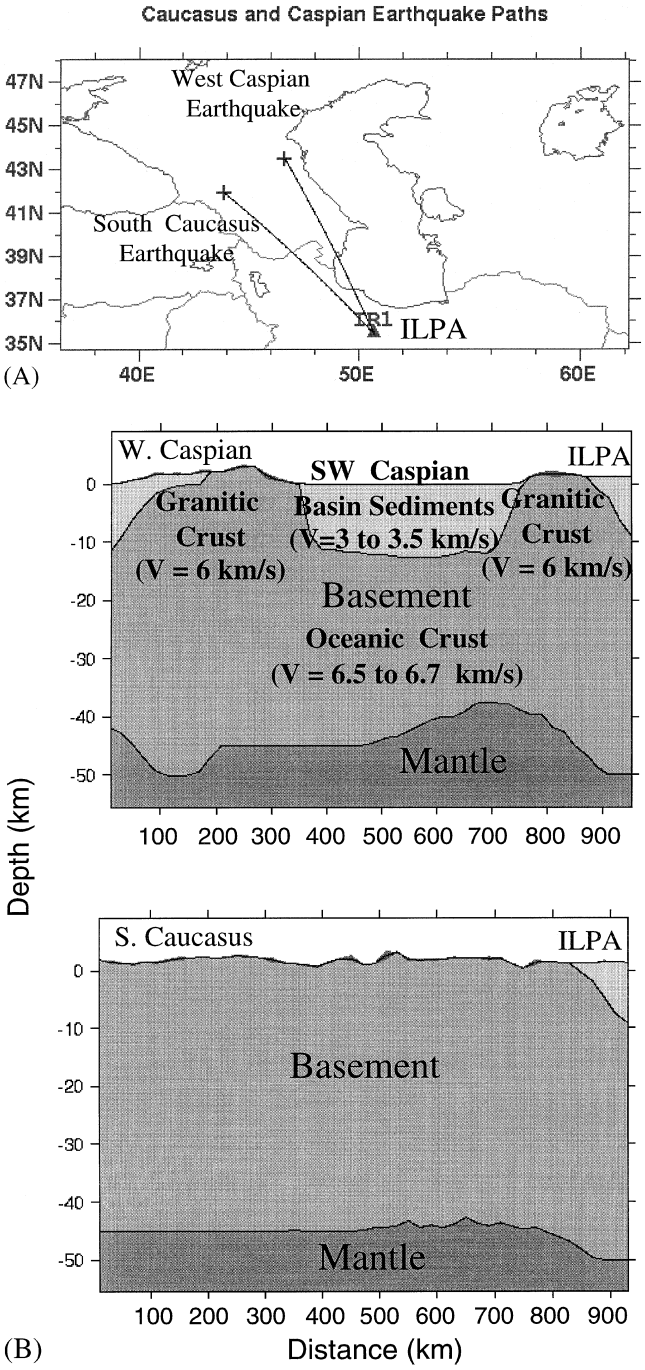
Caucasus and Caspian Earthquake Paths
West Caspian
Earthquake
South Caucasus
Earthquake
ILPA
47N
45N
43N
41N
39N
37N
35N
40E
50E
60E
(A)
W. Caspian
SW Caspian
Basin Sediments
(V=3 to 3.5 km/s)
ILPA
Granitic
Crust
(V = 6 km/s)
Granitic
Crust
(V = 6 km/s)
Basement
Oceanic Crust
(V = 6.5 to 6.7 km/s)
Mantle
Depth (km)
0
-10
-20
-30
-40
-50
100 200 300 400 500 600 700 800 900
S. Caucasus
ILPA
Basement
Mantle
Distance (km)
(B)

Figure 19A, B

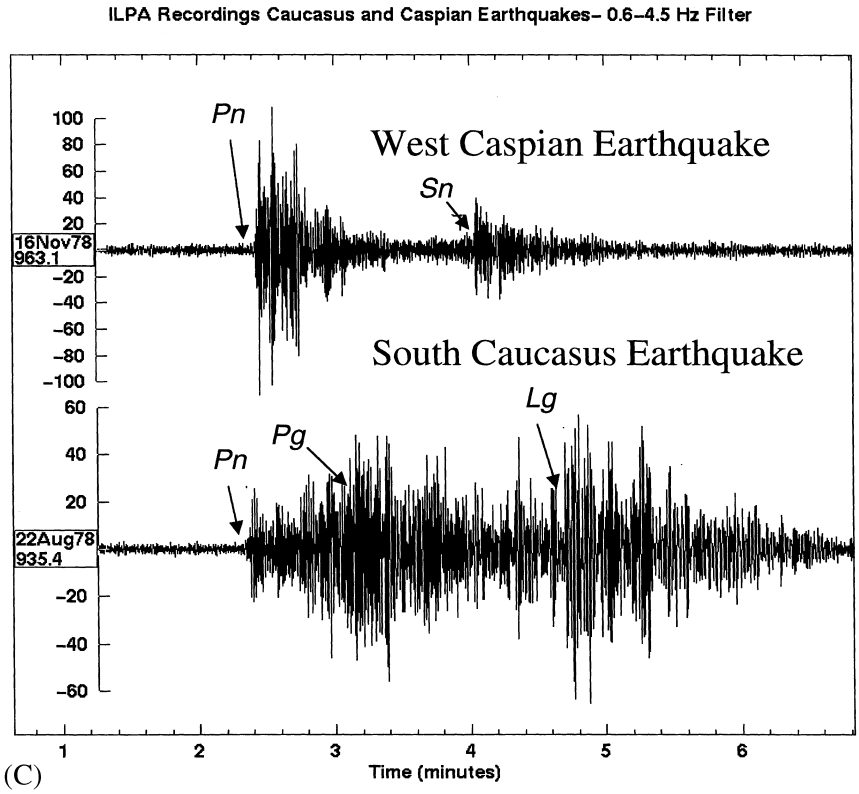

Figure 19
(A) Propagation paths from events west of the Caspian Sea with blocked and unblocked paths. (B) Crustal cross sections for the unblocked (blocked) and unblocked (bottom) paths. (C) Comparison of the ILPA IR1 recordings of the blocked (top) and unblocked waveforms.

The structure is the same as the Barents and North Caspian Basins in that the upper-crustal heterogeneity caused by the sedimentary basins may cause the *Lg* blockage across these regions. Evidently, whether or not there is oceanic crust beneath the sedimentary basin is immaterial to the *Lg* blockage. ZHANG and LAY (1995) modeled *Lg* propagation through various ocean-basin earth models and showed that the primary cause of poor *Lg* propagation across the oceanic crust is the thinness of the crust itself, not the composition. They demonstrate that a typical 6-km thick oceanic crust cannot accommodate a sufficient number of modes that can combine to produce *Lg*, as is possible in a 15-km thick continental crust. Even for mixed oceanic/continental crust, with the requisite 100 km of oceanic crust for *Lg* blockage, it is the thinness of the oceanic segment that blocks the *Lg*.

In the case at hand of the Southern Caspian Basin, even if there are subducted oceanic crustal rocks of the Tethys present beneath the basin, Figure 19(B) shows that

the crust has uniform thickness on the order of 45 km. However, it would appear that the large velocity contrast between the sediments of the contained sedimentary basin and the surrounding crust, whether continental or oceanic, could trap the *Lg* waves in the basin and may explain the blockage of *Lg* across the southern Caspian Sea. Moreover, *Lg Q* may be low in these sediments as well which can cause the anomalous attenuation of *Lg* waves that cross the basin. Thus, this analysis suggests that it is the low velocity and low *Q* sediments in the basin, rather than the high velocity oceanic rocks in the crust under the basin, that are responsible for *Lg* blockage.

Mediterranean/Levantine Basin

We show one final region, the Eastern Mediterranean/Levantine Basin, where *Lg* blockage is associated with a sedimentary basin although with considerably different crustal structure than the regions discussed above. Figure 20 presents a map of propagation paths for earthquakes in Syria, Jordan, Israel, and Lebanon recorded at the Mednet station Kottyama, Egypt (KEG). The source parameters of the earthquakes are listed in Table 5. Most of these events were located along a region defined by the Jordan-Dead Sea transform fault system that separates the Arabian and Sinai plates. Tectonically, the Dead Sea transform system has evolved since mid-Cenozoic time as a result of the breakup of the Arabian plate from the African plate (AMBRASEYS and BARAZANGI, 1989). The system includes the pull-apart basins of the

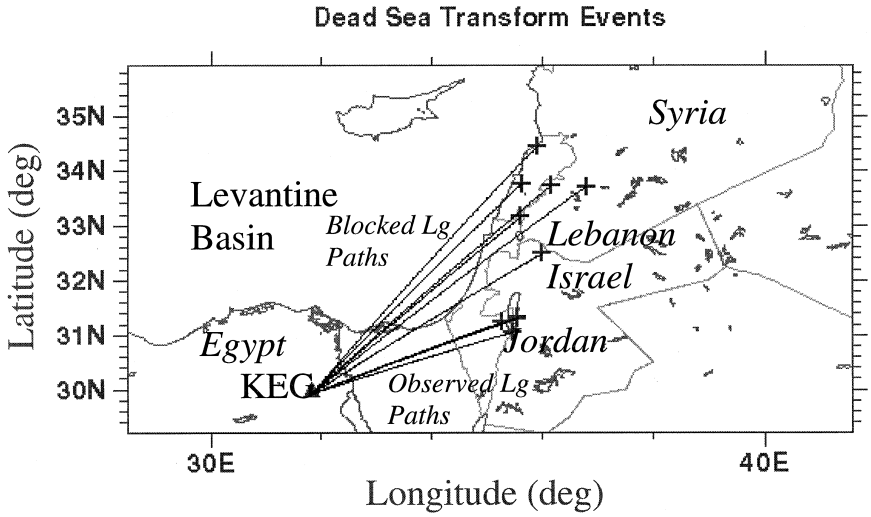

Figure 20
Map showing the propagation paths from events along the Dead Sea Transform to the Egyptian Mednet station at Kottyama (KEG).

Table 5

NEIS event parameters for events on the Dead Sea Fault recorded at KEG

Date	Time	Latitude	Longitude	Depth	Magnitude
06/23/91	13:02:22	31.312	35.557	10	–
09/28/91	00:43:07	31.048	35.464	10	3.9 (M_L)
10/18/91	16:48:50	33.702	36.792	10	4.9 (M_b)
07/29/92	05:30:43	32.489	36.007	10	3.3 (M_L)
03/09/92	19:54:27	34.454	35.925	5	4.2 (M_b)
09/07/92	02:57:52	31.298	35.551	10	3.7 (M_L)
04/24/93	03:45:14	33.154	35.615	24	3.6 (M_L)
07/30/93	11:46:20	33.727	36.173	33	3.7 (M_L)
11/12/93	20:34:54	33.758	35.628	10	4.2 (M_L)

Sea of Galilee and the Dead Sea and extends as far north to the Ghab and Yammouneh faults in Syria and south into the Gulf of Aqaba.

The crustal structure in the region is known to be quite variable because it was formed by the convergence of a number of displaced terranes (BEN-AVRAHAM and GINZBURG, 1990). The eastern Mediterranean Sea is underlain by the quaternary Levantine Sedimentary Basin. Seismic refraction surveys of the basin have inferred seismic velocities of 1.5 to 2.1 km/sec in the sediments in the eastern part of the basin, extending to depths of 8 to 10 km depth underlain by velocities of 4.1 to 4.5 km/sec. The adjoining Galilee-Lebanon, Samaria, and Negev regions have very different crustal structures, perhaps thinner crust, and the seismic velocities in the upper crust range from 3.7 to 6.2 km/sec. As shown in Figure 20, all the events occurred east of the Levantine Basin, however the great-circle propagation paths from the northern events in Syria and Lebanon to KEG cross the eastern part of the Levantine Basin.

A record section of these events, with vertical component waveforms filtered from 0.6 to 6 Hz, is shown in Figure 21. The most notable observation in this plot is the apparent blockage of *Lg* between 388 km and 488 km distance from KEG.

Figure 22 shows a comparison crustal cross sections for the unblocked and blocked paths. The blocked paths are associated with the paths that cross the Levantine Basin. However, Figure 22 shows that the Moho is elevated by as much as 15 km beneath the basin, and water depths approach 4 km.

The record section in Figure 21 also reveals that *Sn* is non-existent for the shorter distance where *Lg* is observed, but is strong at the greater distances where *Lg* is blocked. Also, *Pg* apparently disappears when *Lg* does, and the *Pn* is more impulsive for the paths where *Sn* is strongest.

These results are consistent with the observation in the Barents Sea and Caspian Sea basins. The *Pg*, *Lg* blockage is associated with paths which cross the sedimentary basin. However, the Levantine Basin has the additional features of 15 km of crustal thinning and 4 km water depths, both of which approach the wavelength of *Lg*.

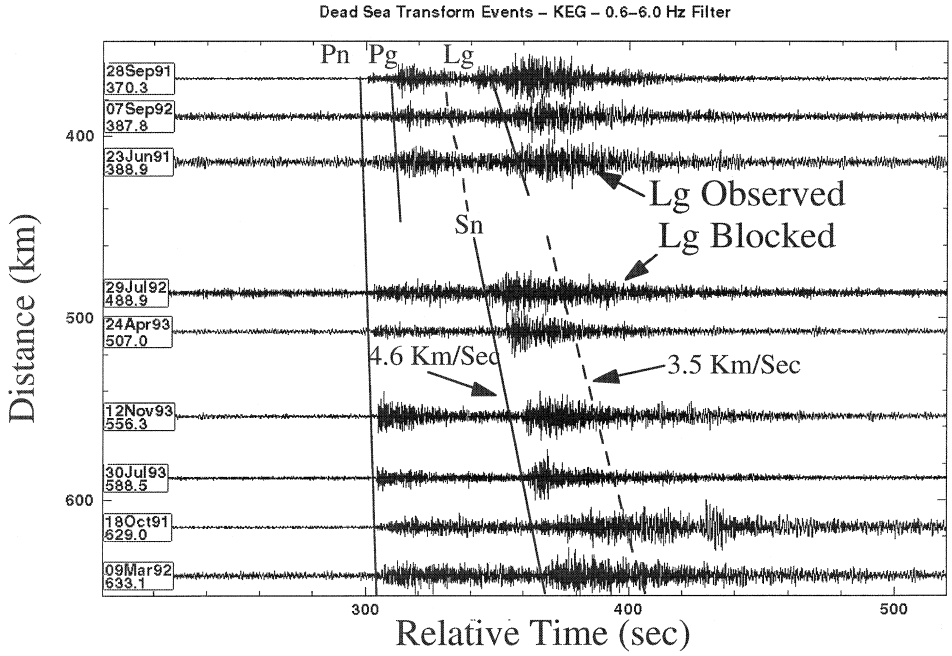

Figure 21
Record section of KEG waveforms, prefiltered from 0.6 to 6 Hz, from the Dead Sea Transform events. Expected times for *Pn*, *Pg*, *Sn*, and *Lg* are indicated.

Basin Capture Model for Lg Blockage

The examples presented above strongly suggest that sedimentary basins block *Lg* waves. The modeling study of *Lg* blockage by CAO and MUIREHEAD (1993) demonstrated that a sedimentary basin structure can partially block *Lg*. However, the crustal structure also included a sudden decrease in the Moho depth and a crustal pinch out. Sudden crustal thinning was also considered by KENNETT (1986) and proposed as a possible explanation of *Lg* blockage. Such structures might explain the *Lg* blockage in the Levantine Basin where the crustal pinch out is very prominent in Figure 22. However, this model would not explain *Lg* blockages in the Barents and Caspian Sea Basins, where Moho depths either do not vary or become greater and the pinch out structures are not apparent.

Also, low Q for *Lg* has also been proposed as a cause of *Lg* blockage, for example, across Tibet (MCNAMARA *et al.*, 1996). The tomographic *Lg*-Q maps of MITCHELL *et al.* (1997), and the cross sections shown in this paper from those maps, do suggest that low *Lg* Q in Northern and Southern Caspian Basins may explain why *Lg* is blocked in these regions, but does not appear to be blocked by the Urals Basin which has higher Q.

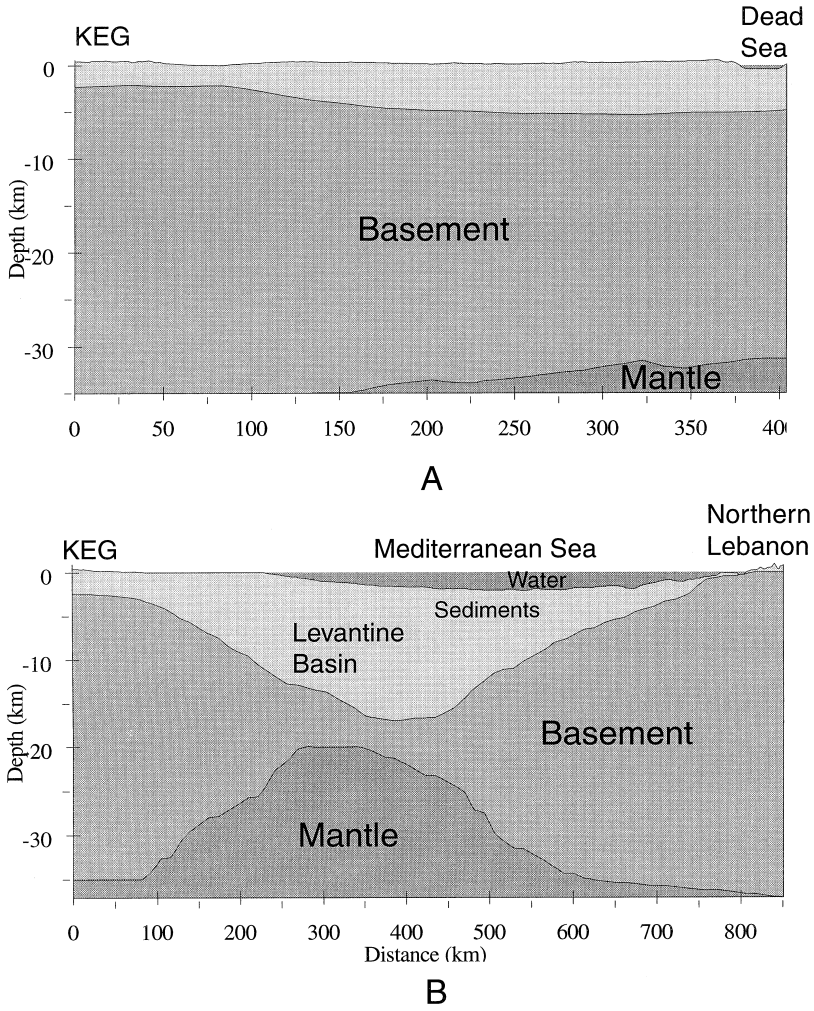

Figure 22
(A) Crustal cross section corresponding to one of the paths from the Dead Sea Transform to KEG where *Lg* is not blocked. (B) Crustal cross section corresponding to a path were *Lg* is blocked.

A mechanism called "basin capture" is suggested to explain the blockage of *Lg* in sedimentary basins that does not require anomalous crustal thickness variations, such as a pinch out. To demonstrate basin capture, we use the representation of *Lg* as the superposition of shear waves, multiply-reflected in the upper crust. The ray-tracing method of KENNETT (1986) has been used to model the interaction of *Lg* with structural boundaries by tracing *S*-type rays through the two-dimensional structure. The phase velocity of the wave is the horizontal component of shear-wave velocity in the upper layer of the velocity model, which is controlled by the shear-wave velocity

in the layer and the takeoff angle of the ray from the source. The phase velocity is assumed to be about 4.5 to 5.0 km/sec for *Sn* and 4.0 to 4.5 for *Lg*. The group velocity is the distance that the wave traverses divided by the travel time. Group velocities are about 4.5 km/sec for *Sn* and 3.5 km/sec for *Lg* waves.

A sedimentary basin like the Barents Basin is modeled as an inverted trapezoidal structure whose top width is 5000 km and bottom width is 2000 km. The basin is assumed to be filled with sediments reaching a maximum depth of 15 km. The shear-wave velocities inside the basin are assumed to be 2.6 km/sec at the top which gradually increases to about 3.46 km/sec at the bottom and sides of the basin. These velocities correspond to compressional velocities of 4.5 km/sec in the sediments and 6.0 km/sec at the sides of the basin. The velocities in between are interpolated by cubic splines. The velocities outside the basin in the granitic layer are assumed to be 3.46 km/sec. The rest of the model is assumed to be a normal, continental structure, with two layers in the crust overlying the mantle.

The source is assumed to be located on the left side of the structure, approximately 500 km from the upper corner of the basin, and the rays travel from left to right. The receiver is assumed to be located somewhere on the right-hand side of the structure outside of the basin. This approximates the situation of the Novaya Zemlya to ARCESS path. The ray-tracing calculations were made using RAY81 (ÇERVENY *et al.*, 1977).

Figures 23(A) and (B) contrast the propagation of an *Lg*-type ray in a structure without (left) and with (right) the sedimentary basin, respectively. Starting with an input phase velocity of 4.9 km/sec, the output group velocity is 3.5 km/sec as expected for *Lg*. As shown, Figure 23(A) on the left, simple shear-wave reverberation in the "granitic" layer, or the upper crust, of the laterally homogeneous structure produces the combination of phase and group velocities expected for *Lg*. Figure 23(B) on the left shows that shear waves that propagate into the lower crust below 15 km, with phase velocity of 4.0 km/sec, would have a group velocity of 3.73 km/sec, which is faster than is expected for first arrival *Lg*. These reverberations may contribute to the later-arriving *Sn* coda. However, shear-wave reverberations in the granitic layer of the crust have phase and group velocities closer to those expected for the first arrival *Lg*.

The presence of the sedimentary basin in the structure severely disrupts the pattern of propagation of the reverberations in the granitic layer wherein the shear waves that compose the *Lg* wave train are effectively captured in the low-velocity sediments of the basin. One effect is that the waves that propagate into the basin are bent closer to vertical by the velocity contrast between the higher granitic velocities (about 6.0 km/sec) outside the basin and the slower, sedimentary velocities (3 to 4 km/sec) inside the basin. Another is that the rays become trapped in the upper layers of the structure. The waves are then guided by the slower velocities in the upper part of the basin structure until they arrive at the other side of the basin. After they submerge back into the homogeneous structure, they have been considerably

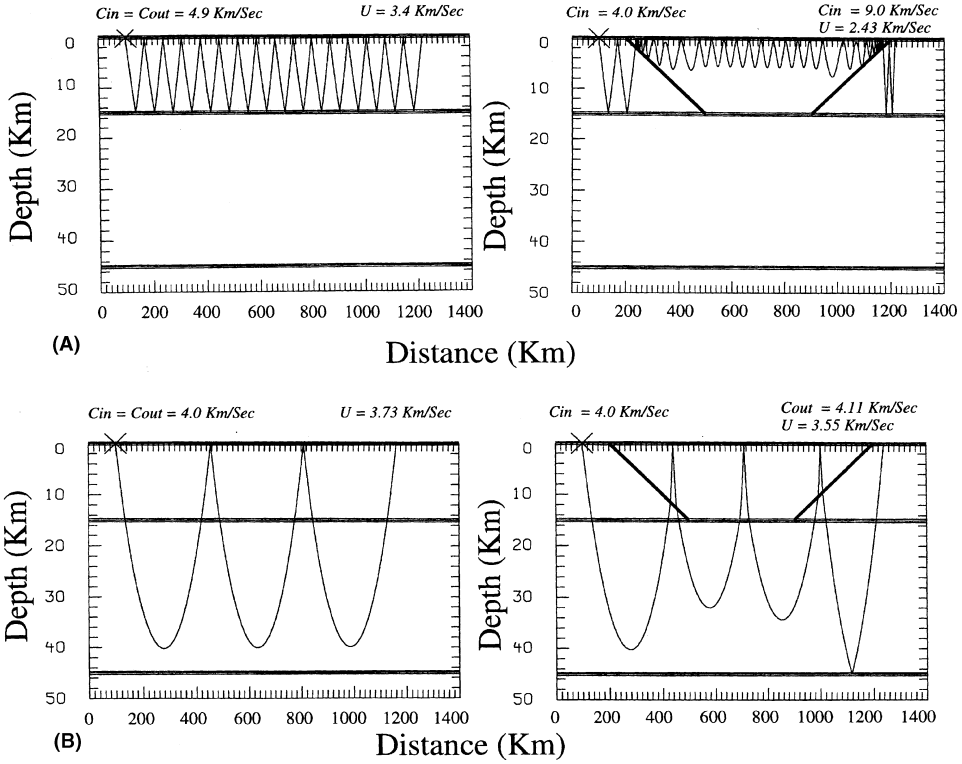

Figure 23A, B

slowed down. In this case the group velocity of the rays comprising *Lg* would only be 2.43 km/sec. Furthermore, the original phase velocity has been greatly altered because of the dipping interfaces between the basin structure and the surrounding homogeneous structure. For the model in Figure 23(B), the *S* wave reverberations, which start out with *Lg* phase velocities, have been converted to steeply dipping rays with phase velocities near 9 km/sec. These phases may become *Sn* type modes or convert to *P* waves. This mechanism might explain how *Lg* waves scatter into *P* and *Sn* coda waves.

Thus, the effect of the basin structure on *Lg* is that shear waves are captured in the upper layers and that direct *Lg* waves are essentially delayed and spread out over decidedly later times. Because of the repeated reverberations in the upper layers and the likely lower *Q* in these layers, the original *Lg* waves would be severely dissipated. Whether the *Lg* is completely dissipated or not depends on the dimensions of the basin through which the *Lg* waves must propagate. The most likely result would be that the *Lg* modes, instead of arriving as a distinct arrival, would be spread out into long coda with amplitudes which diminish with time. This example shows that it is lateral heterogeneity in the upper crust which is required to block the propagation of

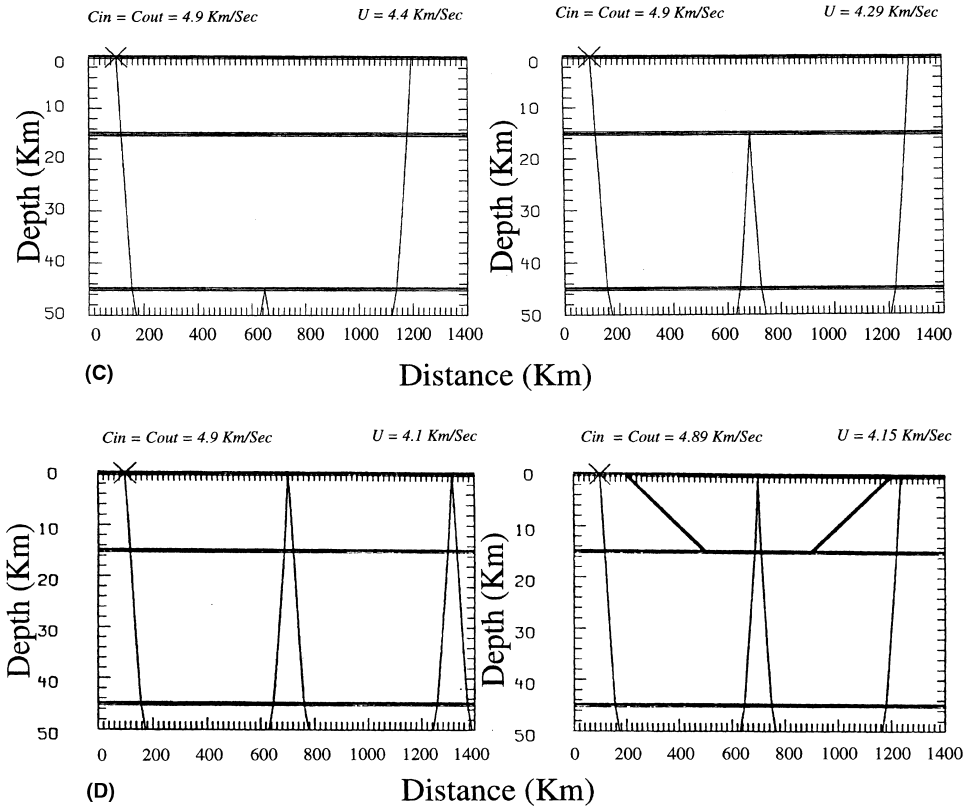

Figure 23

(A) Ray plots of shear-wave reflections in a crustal granitic layer that give propagation properties of *Lg*-type waves. Homogeneous path is shown on the left and effect of a sedimentary basin in the path is shown on the right. (B) Ray plots of shear waves refracting through the lower crust. Homogeneous path is shown on the left and the effect of a sedimentary basin is shown on the right. (C) Rays paths of diving shear waves in the mantle, corresponding to *Sn*-type waves, that propagate below any lateral heterogeneity in the upper crust. (D) *Sn*-type waves that pass twice through the upper crust. Effect of sedimentary basin is shown on the right.

Lg, and which effects in the lower crust or at the Moho would have little effect on *Lg*. Figure 23(B) on the right indicates that shear waves propagating through the entire crust would be delayed by the basin and produce group velocities of close to 3.55 km/sec. However, they are not as strongly affected as shear waves propagating in the upper crust, and the main effect of the basin would be to stretch out the *Sn* coda wave arrivals to later times.

Two examples of *Sn* type propagation are shown in Figures 23(C) and (D), where *Sn* is modeled as a diving wave in the lower crust and upper mantle. No attempt has been made to model decreased depth of the Moho, which has been observed in the Barents Basin. However, if *Sn* is primarily composed of diving waves in the upper

mantle, they would not be greatly affected by such an effect since it is mainly controlled by the structure of the upper mantle, although Moho depth variations may change the group velocities of *Sn* modes which bounce off the bottom of the Moho. Also, the *Sn* wave would propagate below the sedimentary basin and be totally unaffected by it.

Figure 23(D) on the right depicts another type of *Sn* propagation which might be affected by the presence of the basin. Shear-wave reverberations which involve the entire crust would produce group velocities of about 4.15 km/sec which are on the lower end of the range expected for *Sn*. However, although this mode would propagate into the basin structure, because of the high-phase velocities of these *Sn* modes and steeper angles of incidence, they are not captured by the basin and essentially propagate through the structure with virtually no blockage effects.

Conclusions

The well-recognized problem of "*Lg* blockage" has been reexamined in terms of the effect of sedimentary basin structures. This study has shown that the three regions where strong *Lg* blockage has been observed, the Barents and Caspian Seas, and eastern Mediterranean regions, are associated with the presence of deep enclosed sedimentary basins where low-velocity sediments replace the granite velocity rocks in the upper crust.

Simple ray-tracing has been used to illustrate a "basin capture" model which explains *Lg* blockage by the sedimentary basin capturing and delaying the *Lg* modes and their amplitudes being reduced by repeated reverberations and scattering within the basin. The ray-tracing study only gives a first-order representation of the propagation of *Lg* through the sedimentary basin. Only the primary rays, i.e., shear waves that reverberate in the crustal granitic layer, were included in the ray-tracing. Actual *Lg* waves consist of many such rays, and undoubtedly some may follow paths that do not pass through the heterogeneous structure. A true modeling of *Lg* should include all possible rays that may show that some of the *Lg* energy can propagate through the heterogeneous structure. The incoherent beam analysis of the Novaya Zemlya events has, in fact, shown that the coda shapes flatten at the expected time of the onset of on-time *Lg* so that *Lg* is not completely blocked. However, the ray plots of the primary rays represent the paths traversed by most of the *Lg* energy, and they will clearly be diverted by the sedimentary basin along the path.

However, other explanations may also be invoked to explain *Lg* blockage, perhaps in combination with the basin capture idea. First, unusually low-Q associated with the sediments may also explain the strong attenuation, as suggested by MITCHELL and HWANG (1987) and MITCHELL *et al.* (1997). Low *Lg* Q has been observed in the Caspian Sea and eastern Mediterranean Sea regions. The fact that the *Lg* Q tomography map for the Barents Region does not reveal low Q may be an

artifact of the inversion process and lack of resolution, as has been pointed out by MITCHELL *et al*. (1997). Second, the crustal pinch out blockage appears to be clearly present in the Levantine Basin.

Also, basin capture cannot completely explain all the observations at NORSAR from the Southern Urals, especially the lack of blockage of *Lg* across the South Urals Basins. The fact that these basins are small and *Lg Q* is high, might be part of the explanation. The lack of *Sn* and *Lg* from the Astrakhan event may be more of a source effect than a blockage effect, since this event was probably detonated in salt in the Pri-Caspian Basin. Source-parameter effects also cannot be completely ruled out for the earthquakes as a cause of the variations in *Lg* amplitude. However, we might expect source mechanism to be less important at high frequencies.

Finally, the question of the utility of *Lg* for event identification in the face of blockages must be addressed. Obviously, *P*/*Lg* amplitude-ratio discriminants cannot be used if *Lg* is blocked by the propagation path. Crustal cross sections, derived from GIS databases such as those at Cornell, may have some predictive value for *Lg* blockage. However, uncertainties in the parameters in these cross sections must be considered when making these predictions. This study has shown that when *Lg* is blocked, *Sn* sometimes appears enhanced. In fact, earthquakes can be identified on the basis of small *P*/*Sn* amplitude ratio when weak or no *Lg* is recorded. Often, however, when *Lg* propagates with high energy, *Sn* is not well observed. This apparent tradeoff, if it can be shown to hold in general, may be related to the way in which the total shear-wave budget from an earthquake is partitioned in the laterally heterogeneous crust. Future studies should address this apparent tradeoff, both experimentally and in models.

REFERENCES

ALVERSON, D. C., COX, D. P., WOLOSHIN, A. J., TERMAN, M. J., and WOO, C. C. (1967), *Atlas of Asia and Eastern Europe to Support Detection of Underground Nuclear Testing*, *Vol II*., *Tectonics*, prepared by the Department of the Interior, U.S. Geological Survey, for the Advanced research Projects Agency.

AMBRASEYS, N. N., and BARAZANGI, M. (1989), *The 1759 Earthquake in the Beak Valley: Implications for Earthquake Hazard Assessment in the Eastern Mediterranean Region*, J. Geophys. Res. *94*, 4007–4013.

BARAZANGI, M. J. (1977), *Relative Excitation of the Seismic Shear Waves Sn and Lg as a Function of Source Depth and their Propagation from Melanesia and Banda Arcs to Australia*, Annali di Geofisica *30*, 385–407.

BAUMGARDT, D. R. (1985), *Comparative Analysis of Teleseismic P Coda and Lg Waves from Underground Nuclear Explosions in Eurasia*, Bull. Seismol. Soc. Am. *80*, 1413–1433.

BAUMGARDT, D. R. (1990), *Investigation of Teleseismic Lg Blockage and Scattering Using Regional Arrays*, Bull. Seismol. Soc. Am. *80*, 2261–2281.

BAUMGARDT, D. R., and YOUNG, G. (1990), *Regional Seismic Waveform Discriminants and Case Based Event Identification Using Regional Arrays*, Bull. Seismol. Soc. Am. *80*, Part B, 1874–1892.

BEN-AVRAHAM, Z., and GINZBURG, A. (1990), *Displaced Terranes and Crustal Evolution of the Levante and the Eastern Mediterranean*, Tectonics *9*, 613–622.

BENNETT, T. J., BARKER, B. W., MARSHALL, M. E., and MURPHY, J. R. (1995), *Detection and Identification of Small Regional Seismic Events*, Final Report, PL-TR-95-2125, S-Scubed, La Jolla, CA.

BERBERIAN, M. (1983), *The Southern Caspian: A Compressional Depression Floored by a Trapped, Modified Oceanic Crust*, Can. J. Earth Sci. *69*, 163–183.

CAO, S., and MUIREHEAD, K. J. (1993), *Finite Difference Modeling of Lg Blockage*, Geophys. J. Int. *115*, 85–96.

CAMPILLO, M., PLANTET, J.-L., and BOUCHON, M. (1985), *Frequency-dependent Attenuation in the Crust Beneath Central France from Lg Waves: Data Analysis and Numerical Modeling*, Bull. Seismol. Soc. Am. *75*, 1395–1411.

ÇERVENY, V., MOLOTKOV, I. A., and PSENÇIK, I. (1977), *Ray Method in Seismology*, Univerzita Karlova, Praha.

CHAN, W. W., and MITCHELL, B. J. (1985), *Surface Wave Dispersion, Crustal Structure, and Sediment Thickness Variations across the Barents Shelf*, Geophys. J. R. Astr. Soc. *80*, 329–344.

CHINN, D. S., ISACKS, B. L., and BARAZANGI, M. (1980), *High-frequency Seismic Wave Propagation in Western South America along the Continental Margin, in the Nazca Plate and across the Altiplano*, Geophys. J. R. Astr. Soc. *60*, 209–244.

CLARKE, J. W., and RACHLIN, J. (1990), *Geology of the Barents Sea Structural Basin*., US Geological Survey, Military Geology Project, Open-File Report, July, 1990.

EROS (Earth Resources Observation Systems) Data Center (EDC) (1996), *GTOPO30 (a Digital Elevation Model)*, United States Geological Survey (USGS).

EWING, M., JARDETSKY, W. S., and PRESS, F., *Elastic Waves in Layered Media* (McGraw-Hill, New York, 1957).

FIELDING, E. J., ISACKS, B. L., and BARAZANGI, M. (1992), *A Geological and Geophysical Information System for Eurasia*, Technical Report No. 2, Cornell University, Ithaca, New York.

GUPTA, I. N., BARKER, B. W., BURNETTI, J. A., and DER, Z. A. (1980), *A Study of Regional Phases from Earthquakes and Explosions in Western Russia*, Bull. Seismol. Soc. Am. *70*, 851–872.

GRANT, L., RYALL, F., HENSON, I., and RIVERS, W. (1996), *Ground truth database for seismic discrimination research*, Proc. of the 18th Annual Seismic Res. Symp. on Monitoring a Comprehensive Test-Ban Treaty, 4–6 September 1996, *PL-TR-96-2153*, Environmental Research Papers, no. 1195 (eds LEWKOWICZ, J. F., MCPHETRES, J. M., REITER, D. T.) pp. 997–1006.

HARJES, H. P., and SEIDL, D. (1978), *Digital Recording and Analysis of Broadband Seismic Data at the Grafenburg (GRF) Array*, J. Geophys. Res. *65*, 511–523.

HARTSE, H. E., TAYLOR, S. R., PHILLIPS, W. S., and RANDALL, G. E. (1997), *A Preliminary Study of Regional Seismic Discrimination in Central Asia with Emphasis on Western China*, Bull. Seismol. Soc. Am. *87*, 551–568.

ISACKS, B. L., and STEPHENS, C. (1975), *Conversion of Sn to Lg at a Continental Margin*, Bull. Seismol. Soc. Am. *65*, 224–235.

JIH, R. S. (1995), *Waveguide Effects of Large-scale Structural Variation, Anelastic Attenuation, and Random Heterogeneity on SV, Lg Propagation: A Finite-difference Modeling Study*, PL-TR-96-2016, Environmental Research Papers *1186*, Phillips Laboratory, Hanscom, AFB, MA.

KADINSKY-CADE, K., BARAZANGI, M., OLIVER, J., and ISACKS, B. (1981), *Lateral Variations of High-frequency Seismic Wave Propagation at Regional Distances across the Turkish and Iranian Plateaus*, J. Geophys. Res. *86*, 9377–9396.

KENNETT, B. L. N. (1986), *Lg Waves and Structural Boundaries*, Bull. Seismol. Soc. Am. *76*, 1133–1142.

KENNETT, B. L. N., GREGERSEN, S., MYKKELTVEIT, S., and NEWMARK, R. (1985), *Mapping of Crustal Heterogeneity in the North Sea Basin via the Propagation of Lg Waves*, Geophys. J. R. Astr. Soc. *83*, 299–306.

KIM, W. Y., AHARONIAN, V., LERNER-LAM, A. L., and RICHARDS, P. G. (1997), *Discrimination of Earthquakes and Explosions in Southern Russia Using Regional High-frequency Three-component Data from the IRIS/JSP Caucasus Network*, Bull. Seismol. Soc. Am. *87*, 569–588.

KNOPOFF, L., SCHWAB, F., and KAUSEL, E. (1973), *Interpretation of Lg*, Geophys. J. Roy. Astr. Soc. *33*, 389–404.

KUNIN, N., GONCHAROVA, N. V., IOGANSON, L. I., SEMENOVA, G. I., USENKO, S. V., and SHEIKH-ZADE, E. R. (1987), *Map of Depth to Seismic Basement*, Institute of Physics of the Earth, Moscow, Russia.

KUNIN, N., GONCHAROVA, N. V., SEMENOVA, G. I., USENKO, S. V., and SHEIKH-ZADE, E. R. (1988), *Map of Depth to Moho*, Institute of Physics of the Earth, Moscow, Russia.

Mc Namara, D. E., Owens, T. J. and Walter W. R. (1996), *Propagation Characteristics of Lg across the Tibetan Plateau*, Bull. Seismol. Soc. Am. *86*, 457–469.

Mitchell, B. J., and Hwang, H. J. (1987), *Effect of low-Q Sediments and Crustal Q on Lg Attenuation in the United States*, Bull. Seismol. Soc. Am. *77*, 1197–1210.

Mitchell, B. J., Pan, Y., Xie, J., and Cong, L. (1997), *Lg Coda Q Variation across Eurasia and its Relation to Crustal Evolution*, J. Geophys. Res. *102*, 22767–22779.

Morozova, I. B., Morozova, E. A., and Smithson, S. B. (1998), *On the Nature of Teleseismic Pn Phase Observed in the Recordings from the Ultra-long Profile "Quartz", Russia*, Bull. Seismol. Soc. Am. *88*, 62–73.

Murphy, J. R., Sultanov, D. D., Barker, B. W., Kitov, I.O., and Marshall, M. E. (1997), *Further Analyses of Regional Seismic Data Recorded from the Soviet PNE Program: Implications with Respect to CTBT Monitoring*, Final Report, PL-TR-97-2141, October, 1997.

Ni, J., and Barazangi, M. (1983), *High-frequency Seismic Wave Propagation beneath the Indian Shield, Himalayan Arc, Tibetan Plateau and Surrounding Regions: High Uppermost Mantle Velocities and Efficient Sn Propagation beneath Tibet*, Geophys. J. R. Astr. Soc. *72*, 665–689.

Piwinskii, A. J. (1981), *Deep Structure of the Earth's Crust and Upper Mantle in the USSR According to Geological, Geophysical and Seismological Data: Dneiper-Donetsk and Pri-Caspian Depressions*, UCID-19203, Lawrence Livermore Laboratory, Livermore, CA.

Rodgers, A. J., Ni, J. F., and Hearn, T. M. (1997), *Propagation Characteristics of Short-period Sn and Lg in the Middle East*, Bull. Seismol. Soc. Am. *87*, 396–413.

Ruzaikin, A., Nersesov, I., Khalturin, V., and Molnar, P. (1977), *Propagation of Lg and Lateral Variations in Crustal Structure of Asia*, J. Geophys. Res. *82*, 307–316.

Seber, D., Barazangi, M., Tadili, B. A., Ramdani, M., Ibenbrahim, A., Sari, D. B., and El Alami, S. O. (1993), *Sn to Sg Conversion and Focusing along the Atlantic Margin, Morocco: Implications for Earthquake Hazard Evaluation*, Geophys. Research Letters, *20*, 1503–1506.

Shapiro, N., Bethoux, N., Capillo, M., and Paul, A. (1996), *Regional Seismic Phases across the Ligurian Sea: Lg Blockage and Oceanic Propagation*, Phys. Earth and Planetary Int. *93*, 257–268.

Shishkevish, C. (1979), *Propagation of Lg Seismic Waves in the Soviet Union*, N-1014-ARPA, February 1979, Rand, Santa Monica, CA.

Sikharulidzhe, I. I. (1964), *The Nature of Lg and Rg and the Investigation of the Structure of the Earth's Crust*, AS Georgian SSR, Transactions of the Geophysical Institute *22*, 57–70.

Texas Instruments (1977), *Iranian Long-period Array*, Final Report, Equipment Group, Texas Instruments, Inc., 8 April 1977.

Zhang, T. R., and Lay, T. (1995), *Why the Lg Phase Does not Traverse Oceanic Crust*, Bull. Seismol. Soc. Am. *85*, 1665–1678.

Zonenshain, L. P., and Le Pichon, X. (1986), *Deep Basins of the Black Sea and Caspian Sea as Remnants of Mesozoic Backarc Basins*, Tectonophys. *123*, 181–211.

(Received July 1, 1999, revised February 16, 2000, accepted April 24, 2000)